GIS and remote sensing based mapping of microtopography and vegetation composition in a boreal mire complex

Nils Helge Havertz

Master thesis • 30 credits
Swedish University of Agricultural Sciences, SLU
Faculty of Forest Science, Department of Forest Ecology and Management
University of Greifswald
M.Sc. Landscape Ecology and Nature Conservation
Master thesis / Examensarbeten, 2023:7 • ISSN 1654-1898
Umeå 2023

GIS and remote sensing based mapping of microtopography and vegetation composition in a boreal mire complex

Nils Helge Havertz

Supervisor:	**Matthias Peichl, Swedish University of Agricultural Sciences, Department of Forest ecology and Management**
Assistant supervisor:	Sebastian van der Linden, University of Greifswald, Institute for Geography and Geology
Assistant supervisor:	Koffi Dodji Noumonvi, Swedish University of Agricultural Sciences, Department of Forest ecology and Management
Assistant supervisor:	Jonas Bohlin, Swedish University of Agricultural Sciences, Department of Forest Resource Management
Examiner, Umeå:	Anneli Ågren, Swedish University of Agricultural Sciences, Department of Forest ecology and Management
Examiner, Greifswald:	Sebastian van der Linden, University of Greifswald Institute for Geography and Geology

Credits:	30 credits
Level:	A2E
Course title:	Master's thesis in Soil Science, A2E – Forest Ecology and Management
Course code:	EX0961
Programme/education:	M.Sc. Landscape Ecology and Nature Conservation, University of Greifswald
Course coordinating dept:	Department of Forest Ecology and Management
Place of publication:	Umeå
Year of publication:	2023
Copyright:	All featured images are used with permission from the copyright owner.
Title of series:	Examensarbeten/SLU, Institutionen för skogens ekologi & skötsel
Part number:	2023:07
ISSN:	1654-1898
Keywords:	Microtopography modelling, remote sensing, boreal mixed mires, Object Based Image Analysis (OBIA), random forest (RF)

Swedish University of Agricultural Sciences
Faculty of Forest Science
Department of Forest ecology and Management

University of Greifswald
Department of Biology
Institute of Botany and Landscape Ecology

Abstract

Small scale variations in mire surface elevation referred to as microtopography are fundamental characteristics of mire ecosystems especially in the boreal region. Microtopography commonly classified into hummocks and hollows play a major role in several ecological, hydrological and biogeochemical processes including vegetation composition and carbon and methane dynamics. This makes microforms a crucial factor to account on when aiming for modeling ecosystem fluxes and monitoring peatland ecosystem change and resilience under shifting climatic conditions. However, quantitively modelling approaches using the technological advantages of remote sensing applications are limited so far and current methods lack of simplicity and straight forward mapping ability.

In this study a new novel and simple modelling approach for classifying mire microtopography, only based on a digital elevation model (DEM), got applied and tested on four study sites of Kulbäcksliden peatland research infrastructure (northern Sweden). Furthermore, a vegetation classification was performed on the same sites using random forest (RF) classifiers with and without microtopography as an input to evaluate the effect of microforms on the classification accuracy results.

The results indicate promising tendencies for the applicability of the new microtopographic approach even though the accuracy results point out an over estimation of hummock and hollow features, which could be resolved by adapting new height thresholds. The highest overall accuracy of for the vegetation classification was reached using all possible input parameters including microtopography. Still only minor improvements can be observed using microtopography with regards to fine resolution spectral data and the need of optimized height thresholds for microtopography.

Keywords: Microtopography modelling, remote sensing, boreal mixed mires, Object Based Image Analysis (OBIA), random forest (RF)

Table of contents

List of tables

List of figures

1. Introduction

1.1 The role of peatlands in the global carbon cycle

Peatlands are globally distributed ecosystems holding approximately 21-25% of carbon that is stored in terrestrial ecosystems, by only covering about 2-3% of the global land surface, which makes them one of the biggest terrestrial carbon reserves (Beyer et al., 2019; Yu et al., 2010). The majority of peatland are found in the subarctic, boreal and temperate zone and only 10% of them exist along the tropics (Nilsson, 2002; Nungesser, 2003). Northern peatlands play an important role when it comes to the storage and release of carbon dioxide (CO2) and methane (CH4) (Shi et al., 2015). However, C and N elements that has been stored over thousands of years in these systems is projected to be vulnerable facing climatic changes (Wu & Blodau, 2013). A deep understanding of the biological and geochemical processes in northern peatlands is required to model and predict their resilience and greenhouse gas balance under projected future conditions.

1.2 Terminology: peatland and mire, fen and bog

The terminologies “Peatland” and “Mire” are very closely related to each other and both belong to the general concept of wetland types (Rydin & Jeglum, 2015). The term “Peatland” was first commonly used in American literature, while “Mire” was first used in Europe (Caldwell et al., 2006). However, Joosten and Clarke (2002) as well as Rydin and Jeglum (2015) have given them slightly different meanings. Mires are primarily defined as a wet terrain dominated by peat forming plants, where peat is being formed and accumulated (Nilsson, 2002). Peatlands are terrestrial ecosystems, in which over centuries net primary production exceeds organic matter decomposition. This leads to the substantial accumulation of a rich and incompletely decomposed organic matter, called peat (Caldwell et al., 2006). Peat is considered as sedentarily accumulated material consisting of at least 30% (dry mass) of dead organic material (Joosten & Clarke, 2002). Although the terms have slightly different meanings, this study will use both terms interchangeably with a preference for the “Mire” terminology considerate as more adequate for the study site.

Mires are often classified based on their morphology, hydrogeochemical conditions and source of water and nutrients, which defines their specific plant communities (Nilsson, 2002). Bogs are ombrotrophic peatlands with an elevated surface over the surrounding terrain, often isolated from laterally moving mineral-rich soil waters (Rydin et al., 2015). Water supply is restricted to rainfall, creating an acidic and nutrient poor environment dominated by sphagnum mosses (Caldwell et al., 2006). Fens on the other hand receive part of their water supply from groundwater and surrounding mineral soils. They can therefore be nutrient rich or nutrient poor depending on their catchment source with implications on their vegetation composition diversity (Rydin et al., 2015). In reality and typically in the mid-boreal zone, mixed peatland complexes can occur containing a mixture of fen and bog patches and their specific subforms (Rydin et al., 1999).

1.3 Mire microtopography

Small scale (<1-<10 m) variations in surface elevation of mires are named microtopography. They often form distinct spatial patterns across these carbon rich landscapes (Couwenberg & Joosten, 2005; Moore et al., 2019). Current definitions of microforms are still based on their elevation relative to the average surface water table and by structural characteristics like vegetation cover, firstly mentioned by Sjörs (1948) (Harris et al., 2020; Korpela et al., 2020).

Hummocks are defined as locally high and relatively dry areas with elevations between 20-50 cm above the lowest surface water level (Korpela et al., 2020; Nungesser, 2003; Rydin, 2015). For most of the time their peat is well aerated and species found here cannot withstand longer periods of flood. The highest hummocks in northern Sweden are often formed by Sphagnum fuscum and in south western Sweden by S. rubellum, S. magellanicum or S. austrii. In between, specific vascular plants like Empetrum nigrum, Drosera rotundifolia and Calluna vulgaris can be found (Rydin et al., 1999).

Hollows are lower flatter areas or shallow depressions, ranging from small spaces between hummocks to larger open spots. They show a close proximity to the water table and are frequently inundated (Pouliot et al., 2011). Plants occurring in hollows are used to being inundated for relatively long periods. Typical Sphagnum species are S. tenellum, S. cuspidatum and S. majus (Rydin et al., 1999). The deepest elevational occurance of hollows can be found along transitional zones to mud bottoms or pools. Pools are small constantly flooded areas along the peatland surface. Mud bottoms are defined as areas of bare peat soil or algae species lacking vascular plants and mainly occur in some hollows (Pouliot et al., 2011).

Intermediate states between hummocks and hollows are called lawns with elevations slightly over the mean water table. Lawns tend to form a more or less flat surface (Rydin et al., 2015). During summer lawns can arise between 5-20 cm over the average summer water table, whereas

during wetter times they are located right above the water surface, often referred to as swimming carpets (Nilsson, 2002). In the hummock- hollow dichotomy they are usually assigned to hollows, also sharing similarities in their vegetation cover. Lawns are densely grown by Sphagnum mosses with cyperaceous plants and grasses in between. In Swedish mires common cyperaceous species on lawns are Eriophorum vaginatum or Trichophorum cespitosum together with Sphagnum balticum, S. tenellum and S. angustifolium as typical Sphagnum moss species (Rydin et al., 1999).

In mire environments with gentle slopes, microtopographic elements can form distinct elongated mosaic patterns typically occurring in aapa mires or northern ribbed fens but also in mixed boreal mire types (Laitinen et al., 2005). Long hummocky structures, functioning as damming ridges are called strings and usually surround greater areas of wet partially mudded partially vegetated areas defined as flarks. These specific types of hummock-hollow features are often some meters wide and 5- 20m long (Joosten & Clarke, 2002; Rydin et al., 1999).

Explanations for the origin and sustenance of microtopographic patterns focus on the feedback mechanisms existing between vegetation, peat and water (Couwenberg et al., 2005). Mire microtopography is connected to water table dynamics. The majority of biological and peat forming processes occur in the uppermost peat layer called acrotelm. It is defined as the layer above the mean water table level occurring during the growing season with a depth usually ranging from 30-70 cm (Ivanov, 1981). The saturation of the peat is defined as the boundary between the acrotelm and the anaerobic water logged catotelm (Nungesser, 2003). In Sphagnum dominated boreal mire ecosystems, the distance to the water table leads to intra- and interspecific changes in peat moss composition. Sphagnum species growing on hummocks are more chemically resistant to decay than those growing on hollows (Mäkilä et al., 2018). Lower rates of decomposition result in a higher net carbon accumulation, surface elevation and hence to the genesis and maintenance of hummocks. Differential decomposition in hollows lead to lower hydraulic transmissivity, which in combination with the close proximity to the catotelm preserve anoxic and moist conditions in hollows (Nilsson, 2002; Nungesser, 2003; Rydin et al., 1999).
In fact, the difference between more anaerobic conditions in hollows and aerobic conditions found on hummocks influence multiple other important biogeochemical and hydrological processes making microtopographical features an essential factor to account on when trying to understand and model mire ecosystems. Especially their differences in carbon and nitrogen fixation and emission are crucial to precisely estimate and predict greenhouse gas fluxes. Hollows and wetter sites in general, show relatively high nitrogen fixation through binding of cyanobacteria as well as CH_4 emission driven by anaerobic decay. On the other hand, slow aerobic decay processes and warmer and drier conditions throughout the year lead to higher CO_2 fluxes exhibited on hummocks (Graham et al., 2020; Mäkilä et al., 2018).

1.4 Modelling and classification of microtopography and vegetation composition

First research attempts focused on conceptualized modelling and qualitative evaluation of complex peatland microtopography and it`s relation to vegetation composition (Nungesser, 2003; Pouliot et al., 2011). The HOllow- HUMmock (HOHUM) model by Nungesser (2003) was one of the first simulations to provide detailed knowledge about hydrologic and biochemical processes to explain microtopography occurrence, resilience and stability, followed by more complex approaches like the DIGI Bog model (Baird et al., 2012; Nungesser, 2003). However, qualitative and visual measurements of vegetation, water table and elevation are subjective and have the potential to produce biased results, making comparisons between different mire sites, with varying morphology and biogeochemical processes difficult. Moreover, these methods lack the ability to produce fine scale results on a larger spatial extend (Moore et al., 2019).

1.4.1 Remote sensing methods for microtopographic modelling

Recent technological advances in remote sensing (RS) methods have overcome the inability to provide highly accurate data with a fine spatial resolution over large areas (Graham et al., 2020). Different remote sensing platforms and sensors are increasingly used in many ecological fields today to provide quantitative data for monitoring and modelling reasons (Martínez Prentice et al., 2021). Data collection by the use of unmanned aerial vehicles (UAV), also called drones, has established in many scientific fields in recent years (Balestrieri et al., 2021). Their applicability fills the gap between terrestrial ground measures, manned aircraft platforms and satellite-based systems (Xiang et al., 2018). In general, remote sensing sensors can be divided into active and passive systems. To date, mapping microtopography has mainly relied on two technologies: light detection and ranging (LiDAR) and structure from motion (SfM) photogrammetry (Kalacska et al., 2021). LiDAR is an active remote sensing technology, meaning that the platform has its own illumination source. LiDAR systems use laser pulses mainly between 800 and 1500nm for terrestrial applications. The measures are based on the exact time it takes for the pulse to return after they are reflected off objects or the ground (Kalacska et al., 2021).

On the other hand, SfM is a passive remote sensing technique depending on sunlight as an illumination source. Spectral sensors can be categorized as either multi- or hyperspectral, depending on the number and width of the spectral bands (Balestrieri et al., 2021). Besides different sensor techniques, platforms ranging from terrestrial scanning over UAV based acquisition up to airborne based scanning have been used in past publications. Choosing a suitable method is study dependent and important to get appropriate outcomes. Acquisition techniques and classification methods applied for modelling microtopography are summarized in Table 1 together with their advantages and disadvantages.

Table 1 Overview of remote sensing methods for classifying peatland microtopography. The applied RS platforms and spatial resolution are presented in the "RS technology" column.

Authors	RS technology	Method Description	Advantage	Disadvantage
Graham et al. (2020)	Terrestrial Laser Scanning (TLS) 0.01 m (spatial resolution)	- Random roughness (RR) and model semivariograms for classification - They introduced three distinct classification models based on elevation distributions, spatial variability, and surface roughness	- TLS produce densest point clouds - Three different approaches for specific purposes	- Inconsistent results for hollows between the approaches - Only Hummock- Hollow distinction (two-class-approach) -Small extent
Graham et al. (2022)	TLS 0.01 m	- Used the Earth system land model (ELM) classification from Graham et al. 2020 - Two-column (Hummock- hollow) approach for classification - Setting elevational thresholds for distinction (hummock- hollow height differential; hummock-hollow horizontal separation)	- Approach calculates three parameters for microtopographic representation: height differential, horizontal separation, proportional cover of each landform -Modelling results used as Land surface model input to estimate carbon fluxes	- Uncertainty of applicability of the ELM approach using other platforms than TLS and for larger scale mapping - Variation in the results for default values of microform height difference and horizontal separation - Two-class-approach
Stoval et al. (2019)	TLS 0.01 m	- Hollows were detected by a digital terrain analysis (DTA) threshold approach - Determination of hollows in the lower 50% of Digital Surface Model or DSM (low slope and elevation) - Hummock segmentation algorithm (TopoSEg) and watershed delineation for hummock detection	- Allows to derive hummock level metrics for each segmented object - Results show that total classification accuracy increased with decreasing resolution until 50 cm DSM - Approach suitable for fine scale resolutions	- Complex hummock determination process - Hummocks and Hollows a classified independently (no relation) - Subjective manual delineations of hummocks as validation data - Two-class-approach
Brubaker et al. (2013)	Airborne Laser Scanning (ALS) 1 m	- Modelled surface roughness and microtopography using four methods: standard deviation (SD) of slope, SD of curvature, SD of residual topography	- One of the first attempts for quantitative microtopographic modelling - First to consider a pit fill metric	- Digital elevation model (DEM) based classification deviates from the findings of the control plots - Coarse spatial resolution, with a suggestion to use higher resolution DEM - Two-class-approach
Korpela et al. (2020)	ALS & SfM UAV 0.1 m	- Measures from both LiDAR and image data were taken to perform linear discriminant analysis (LDA) and random forest (RF) for classification purposes - Calculation of several input parameters (Standard deviation of surface roughness Hummock index, Depression Index, Textual measures…)	- Classification based on multiple parameters - use of fine resolution DEM - Takes advantage of both LiDAR and image based Red, Green, Blue (RGB) data	- Relatively complex and time consuming approach - Ground truth required - Eight-class approach mixing microforms with vegetation might be to detailed and confusing
Kalacska et al. (2021)	ALS & SfM UAV 0.1 m	- Used a pixel based random forest classifier with the two classes hollow and hummock based on their normalized height value - Compare the LiDAR and RGB images as input data	- Good comparison between both acquisition methods	- Two-class-approach - Results focus mainly on differences between LiDAR and Image data
Lovitt et al. (2017)	SfM UAV 0.02 m	- Generated a smoothed digital terrain model DTM by applying a low pass filter - Pixel- based density slicing approach to detect hummocks and hollows - Results used in CH4 emissions estimations	- Only RGB data based approach - Relatively simple - Used as input parameter for CH_4 flux modelling	- Confusion in transition zone between hummock and hollows - Classification adaptation towards more classes could be difficult to implement- Classification relies on average elevation

Moore et al. (2019)	SfM UAV 0.03 m	- Studied the height distribution and variability of 50 random plots using Gaussian mixed models	- Geostatistical description of microtopographic variations in peatlands	- Microtopography showed contrary to their assumption of a non-bimodal distribution, divagating from Graham et al. 2020 -Small plot sizes and from that parametric microform estimation for the whole area - Removed vegetation in the field before the drone flights - Two-class-approach

Graham et al. (2020,2022) and Stoval et al. (2019) generated digital elevation models (DEM) from dense point clouds acquired by terrestrial laser scanning (TLS). Terrestrial Laser scans can produce the densest point clouds of all published methods but on the other hand, they are limited to a certain spatial extent and dependent on the accessibility of the study site. Airborne LiDAR data used by Brubaker et al. (2013) and Korpela et al. (2020) have developed a lot throughout the years which is also reflected in the spatial resolution of DEM between these two studies. Kalacska et al. (2021) stated that airborne LiDAR (ALS) delivers highly accurate topographic results until a spatial resolution of > 10 cm. At finer resolutions SfM UAV delivers the most promising results. Lovitt et al. (2017), Moore et al. (2019) used SfM UAV based techniques for their data collection. The image data captured by drones have relatively high pixel densities. However, pixels that do not represent the ground must be removed to produce a ground dense point cloud before DEM generation and SfM UAV is generally considered to be more sensitive to ground vegetation than LiDAR data (Kalacska et al. 2021).

Concerning the classification methods, it is pointed out, that with exception of Korpela et al. (2020), all previous studies are limited to a binary classification between hummocks and hollows. However, Lovit et al. (2017) conclude that including a third intermediate class would provide a more realistic modelling result, by minimizing the errors that occur in the transition zone between hummocks and hollows. Methods used by Korpela et al. (2020) and Stovall et. (2019) require several comprehensive input and/or training features and are based on complex parametric models like Gaussian mixed or non-parametric decision tree classifiers. Furthermore, modelling attempts by Graham et al. (2020,2022) and Moore et al. (2019) focused on smaller plot levels did not aim to be applicable over larger areas. Additionally, most methods are often dependent on ground truth data collected in the field, even for the classification step, which makes it difficult to apply in remote and inaccessible areas in upscaling/regional studies. The two mainly used variables are elevational thresholds and surface roughness measures. Lovitt et al. (2019), relied on average elevation as parameter to distinguish between microtopography features, which shows its limitation to surface variability and larger mire extents. The potential of using pit filling algorithms for Hollow identification first mentioned in Brubaker et al. (2013) has not been explored further in recent years. Graham et al. (2020) highlighted the importance of choosing between different approaches suiting for specific purposes. The methods stated here point out a lack of simplicity, straight forward mapping ability and are mainly based on a binary classification only considering hummocks and hollows.

1.4.2 Remote sensing methods for vegetation classification

Compared to microtopography modelling, vegetation classification methods are better developed, studied and established in different fields. Passive remote sensing sensors of different spectral resolution are more frequently used for non-forest vegetation classification purposes even though several studies exist using active sensors like LiDAR data as an additional input for modelling improvement (Beyer et al., 2019; Korpela et al., 2020). Unsupervised and supervised classification algorithms are the two broadest concepts to describe classification methods (Villoslada et al., 2020).

Unsupervised classification methods cluster pixels into relatively homogenous classes of similar spectral signatures. It is a rather simple and quick approach that does not require specific detailed knowledge of the study site. On the other hand, this methodology struggles to compute classes related to different plant communities and is in general limited to more or less homogenous areas with fewer classes (Villoslada et al., 2020).

In a supervised classification the producer guides the image processing by creating training sample areas to direct the classification process. The training pixels can be used to provide an accurate prediction of the exact location of certain plant communities. The classifier then compares the training signatures with the pixels of the image data to assign it to a specific class. Parametric classifiers rely on statistical models like “Minimum-Distance-to-Means” or “Gaussian Maximum Likelihood”, whereas non-parametric classifiers use decision tree approaches like Random forest classification (Lillesand et al., 2008). A central question is how to deal with the spectral range that each plant community possesses. A variety of methods exist for analyzing the variability of spectral reflectance inside a plant community.

Pixel-based image analysis (PBIA) is performed by assigning pixels to a class fundamentally by referring to the spectral similarities. It was the first applicable concept but shows difficulties dealing with the rich information content of high-resolution data (Sibaruddin et al., 2018). However, in recent years another method has proven applicability called object-based image analysis (OBIA). In cases where homogenous vegetation patches are present and represent plant communities larger than pixel size this method shows advantages compared to PBIA (Martínez Prentice et al., 2021). In OBIA, image segmentation is the first step to create objects containing spatial entities composed of homogenous values, on which the afterwards applied supervised or unsupervised classification is based (Martínez Prentice et al., 2021). The segmentation is usually based only on the spectral values from multispectral orthomosaics. However, parameter generated from LiDAR based DEMs have proven applicability as additional inputs to improve classification results. The interaction between only imaged based OBIA on mire vegetation classification and the incorporation of elevational data has been not been studied in detail yet.

1.5 General study aim

The overall aim of this study is to develop and evaluate a new novel and simple modelling approach for classifying mire microtopography in a boreal mire complex, requiring only a DEM as input and basic GIS operations. In a second step, the relevance of microtopography for vegetation classification accuracy was tested by carrying out an object based image analysis (OBIA) using multispectral data collected by UAV, with and without microtopography as a variable.

1.6 Research questions

The specific research questions addressed are:

- How accurate and applicable is the novel DEM-based approach to model mire microtopography?
- Does incorporating microtopography improve the accuracy of mire plant community classification?

2. Methods

2.1 Site description

The study took place at the Kulbäcksliden Research Infrastructure (KRI), which is a research station for studying ecology, hydrology, biogeochemistry and atmosphere- ecosystem gas exchanges in northern peatlands (Dodji Noumonvi et al., 2023). The KRI is located near the municipality of Vindeln in the northern Swedish province of Västerbotten, on an elevated land between the rivers Umeälven and Vindelälven (Figure 1). Four natural fens (Degerö Stormyr, Stortjärn, Hålmyran and Hälsingfors) were included in this study. Each site is equipped, among other installation, with an Eddy covariance flux tower for measuring land-atmosphere exchanges of greenhouse gases, and a suite of meteorological instruments. A network of boardwalks limits disturbance to the mires while facilitating accessibility. Coordinates of the four flux towers and catchment area of the sites are presented in Table 2 (Dodji Noumonvi et al., 2023).

Table 2 Geographical coordinates of the different mire sites (Dodji Noumonvi et al., 2023).

Site	**Degerö**	**Stortjärn**	**Hålmyran**	**Hälsingfors**
Longitude (° E)	19.556543	19.563810	19.569240	19.551496
Latitude (° N)	64.182029	64.174977	64.159996	64.159555
Altitude (m.s.l.)	265.659	268.890	290.117	291.752
Area (ha)	273	30	33	65

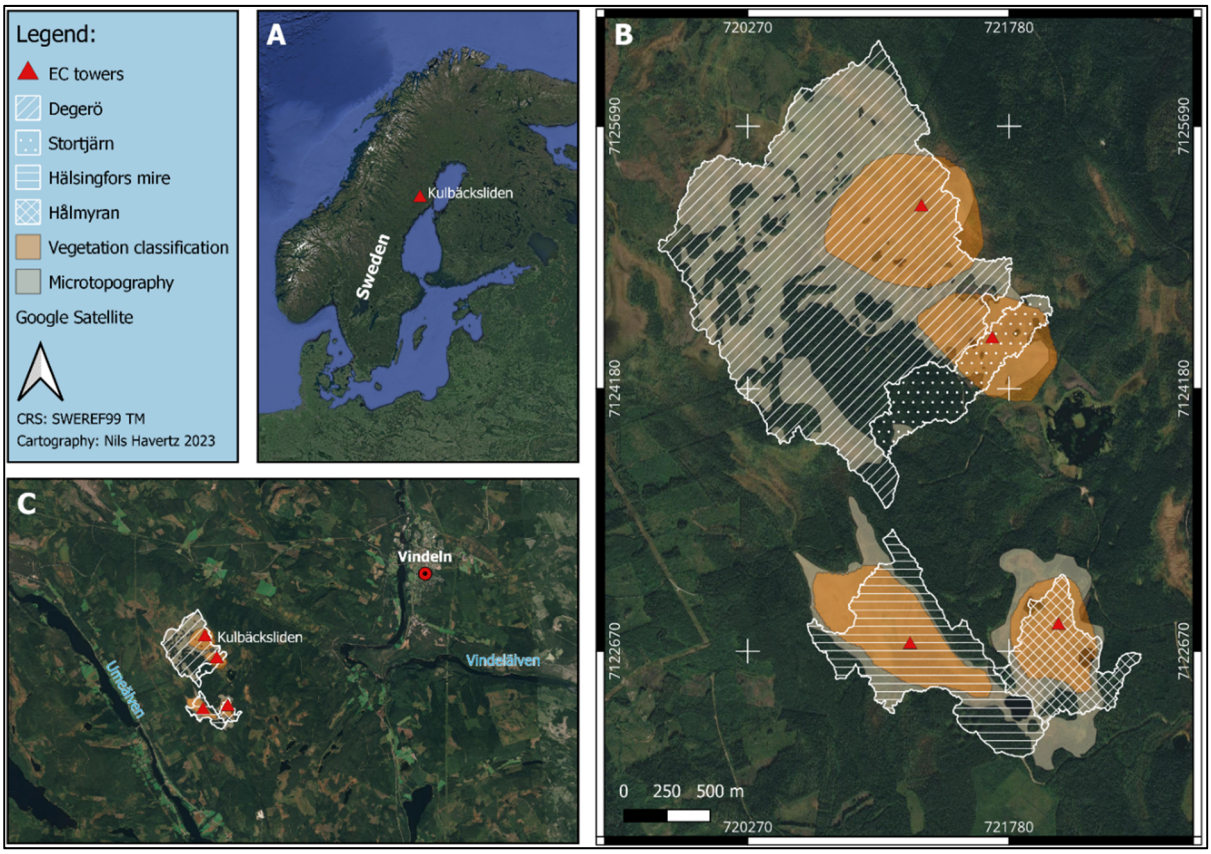

Figure 1 Study area location, catchment area extents and extents covered by microtopography modelling and vegetation classification. Microtopography was modelled for the four catchments, excluding the mineral soils, and vegetation classification only covered the main sites around the flux towers.

2.2 Data acquisition and pre- processing

An existing DEM derived from a 2019 airborne LiDAR data (Riegl VQ-1560i-DW, 532 nm and 1064 nm) covering the entire KRI area served as input data for microtopography modeling. From an original average point density of 20 points per m^{-2}, the existing DEM has a spatial resolution of 0.5 m x 0.5 m (Dodji Noumonvi et al., 2023).

Multispectral UAV images acquired on September 1st and 2nd 2022 at each mire site were used for vegetation classification. The data was acquired using a DJI Phantom 4 multispectral UAV from a height of 55 m above ground level (a.g.l.), and processed in Agisoft Metashape, version 2.0.0 (AgiSoft Metashape Professional, 2022) and Orfeo ToolBox, version 8.1.1 (Grizonnet et al., 2017), producing orthomosaics with a 3 cm ground pixel resolution (Dodji Noumonvi et al., 2023; Ericson et al., 2021). The DJI Phantom 4 multispectral camera enables the acquisition of 5 band images (Blue: 450 nm ± 16 nm, Green: 560 nm ± 16 nm, Red: 650 nm ± 16 nm, Red Edge: 730 nm ± 16 nm, and Near-InfraRed: 840 nm ± 26 nm).
The DEM-based study area for microtopography is overall larger than the extent of the UAV-based data for vegetation classification. The microtopography modelling was performed on two

sub-areas, consisting of Degerö Stormyr-Stortjärn on one hand, Hålmyran-Hälsingfors on the other hand. Vegetation classification however was performed for each of the four study sites individually (Figure 1).

In November 2021, a field inventory was conducted during which different vegetation species were described at more than 50 locations per site, based mainly on the Finnish mire classification system by Eurola et al. 1991 (Dodji Noumonvi et al., 2023; Ericson et al., 2021; Eurola & Virtanen, 1991). Regions of interest (ROI) were drawn from this inventory data and served as ground truth (for training and validation) for the vegetation classification, based on 5 vegetation groups, to which 2 additional classes were added (Table 3).

Table 3 Vegetation groups (visualized in Figure9) resulting from the field inventory data, important plant species and brief group descriptions. Graphic adapted from (Dodji Noumonvi et al., 2023).

Group	Description	Main species
1	Lawns dominated by short sedges and Sphagna	*Eriophorum vaginatum,Trichophorum caespitosum,Carex pauciflora, Andromeda polifolia, Oxycoccus palustris, Sphagnum angustifolium, S. balticum, S. medium, S. rubellum, S. compactum, S. papillosum*
2	Hollows/Carpets dominated by short sedges and Sphagnum subg. Cuspidata	*Eriophorum vaginatum, Trichophorum cespitosum, Scheuchzeriapalustris, Andromeda polifolia, Oxycoccus palustris* *A closed carpet of Sphagnum subg. Cuspidata (S. balticum, S. majus, S. lindbergii, S. jensenii)+ S. papillosum or S. compactum*
3	Hollows/Mud or loose bottoms, tall sedge fens	*Pinus sylvestris, Betula nana, Andromeda polifolia, Calluna vulgaris, Empetrum nigrum, Oxycoccus microcarpus, Vacciniumuliginosum, V. vitis-idaea,Eriophorum vaginatum, Rubus chamaemorus, Sphagnum angustifolium, S. fuscum, S. medium, S. rubellum, Pleurozium schreberi, Cladonia mitis, C. stygia*
4	Hummocks and sparely treed mires	*Pinus sylvestris, Betula pubescens, Picea abies, Betula nana, Andromeda polifolia, Empetrum hermaphroditum, Ledum palustre,Oxycoccusspp.,Vaccinium myrtillus, V. uliginosum, V. vitis-idaea Eriophorum vaginatum, Carex globularis, Dactylorhiza maculata, Rubus chamaemorus, Sphagnum angustifolium, S. divinum, S. russowii,Polytrichum commune, Pleurozium schreberi, Hylocomium splendens, Dicranumspp., Cladoniaspp., Carex rostrata, Sphagnum angustifolium, S. fallax, S. flexuosum, S.riparium*
5	Mire forests including high hummocks	*Pinus sylvestris, Betula pubescens,Picea abies, Calluna vulgaris, Empetrum hermaphroditum., Linnaea borealis, Vaccinium vitis-idaea, V.myrtillus,V. uilginosum, Deschampsia flexuosa, Polytrichum spp., Hylocomium spledens, Pleurozium schreberi, Ptilium crista-castrensis, Barbilophozia lycopodioides, Cladonia spp.*
6	Boardwalks and artificial structures	-
7	Open waters	-

2.3 Microtopography modelling

The entire microtopography modelling was performed in the opensource GIS software QGIS, version 3.28.2 (QGIS Development Team, 2023). In order to automate the workflow and allow reproducibility and reusability, a graphic model was developed using the "Graphic modeler" in QGIS as well as a python script using the python Integrated development environment Spyder (Spyder Doc Contributors, 2023). The python script and the graphic model are accessible at https://github.com/schneider0815/Microtopography-Script.git.

In a first step, a mask layer was created excluding all mineral soils and open water areas from the DEM. The main modelling workflow is based on two initially separated sub steps both based on the input DEM (Figure 2).
In both sub steps the "Fill Sinks" module proposed by (Wang & Liu, 2006) was used to identify and fill surface depressions in digital elevation models (Figure 2, Figure 3). "Fill sinks" is made available in QGIS through SAGA-GIS, and the algorithm was originally made for water flow directions and watershed basins applied in many hydrologic applications dealing with high resolution DEM. By introducing a spill elevation concept and integrating a prior queue data structure into a least-cost search algorithm, Wang & Liu (2006) developed an efficient approach identifying and filling surface depressions in massive DEM inputs. The tool was applied by setting a minimum slope of 0.00001 degrees. The minimum slope preserves a downward slope from cell to cell along the flow path. The choice of a value close to zero instructs the algorithm to fill all cells up to the spill elevation which results in flat areas (Conrad et al., 2015).
Hollows were detected by subtracting the original DEM from the filled one, and all pixels that were filled above a threshold of 0.00001 m were classified as hollows. Hummocks where identified by running a similar process but inverting the original DEM beforehand as described in Equation 1.

$$Inverted_{DEM} = (DEM * (-1)) + Max\ Value \quad \text{(Eq.1)},$$

Equation 1 Where Max Value is the highest altitude in the DEM.

The inversion flips the DEM upside down, hence turning hummocks into depressions, which could then be filled by the "fill sinks" tool. The hollow layer is coded 1 for hollow and 0 for non-hollow, while the hummock layer is coded 2 for hummock and 0 for non-hummock. By summing up the two layers with the raster calculator, a four classes (0 – 3) raster layer is obtained (Figure 2, Figure 3). In the resulting layer, class 0 represents lawns, class 1 represents hollows (pixels filled only in the original DEM), class 2 represents hummocks (pixels filled only in the inverted DEM) and class 3 represents pixels filled in both the original DEM and the inverted DEM. Class 3 pixels are considered to be either small hollow-like depressions on hummocks or hummock-like features in hollows (Figure 3). Their occurrence was further evaluated to assess their relevance as a distinct class.

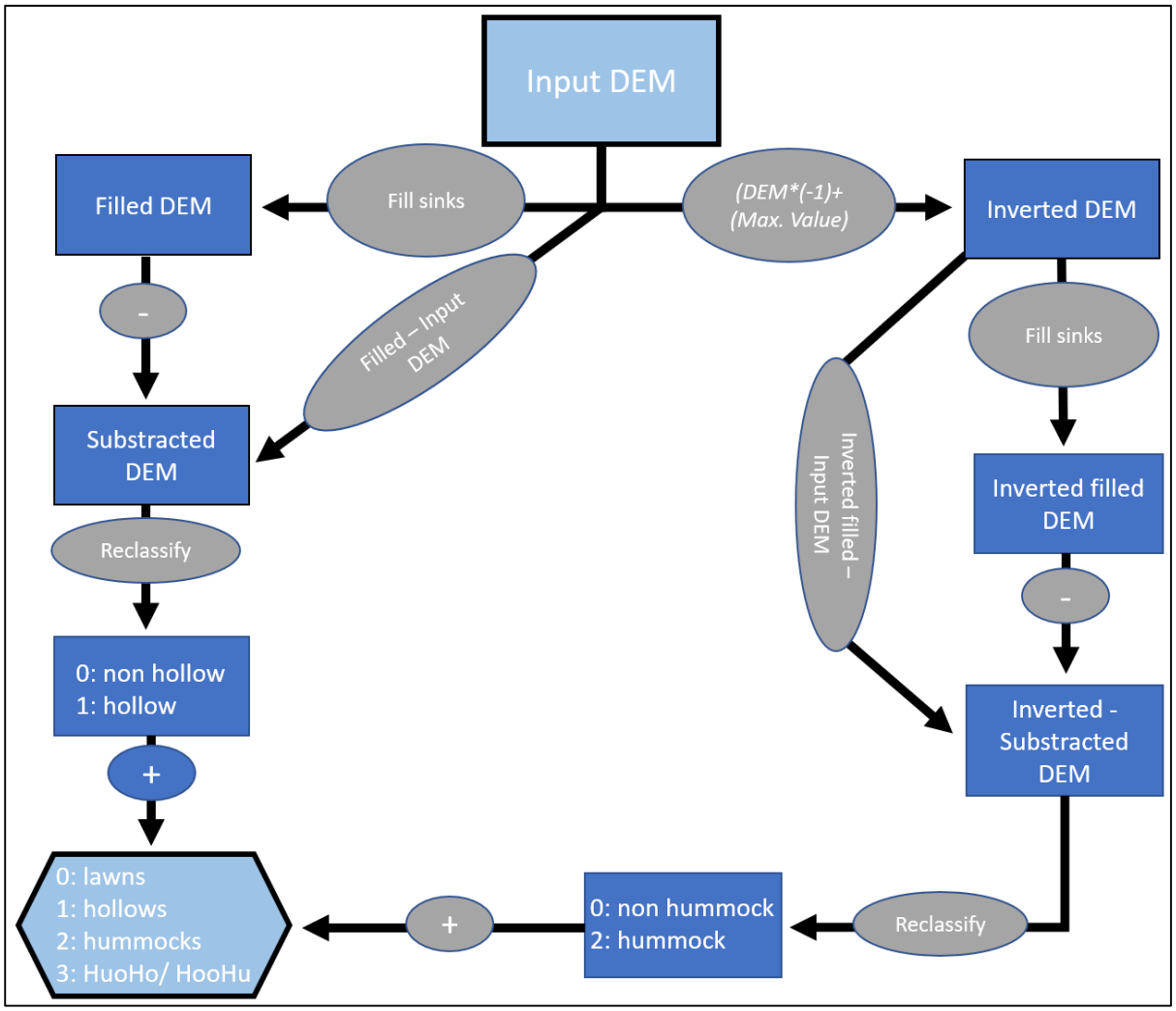

Figure 2 Microtopography modeling workflow. Tools and processing steps as elliptic gray features. Resulting layers in dark blue squares. In- and output in light blue.

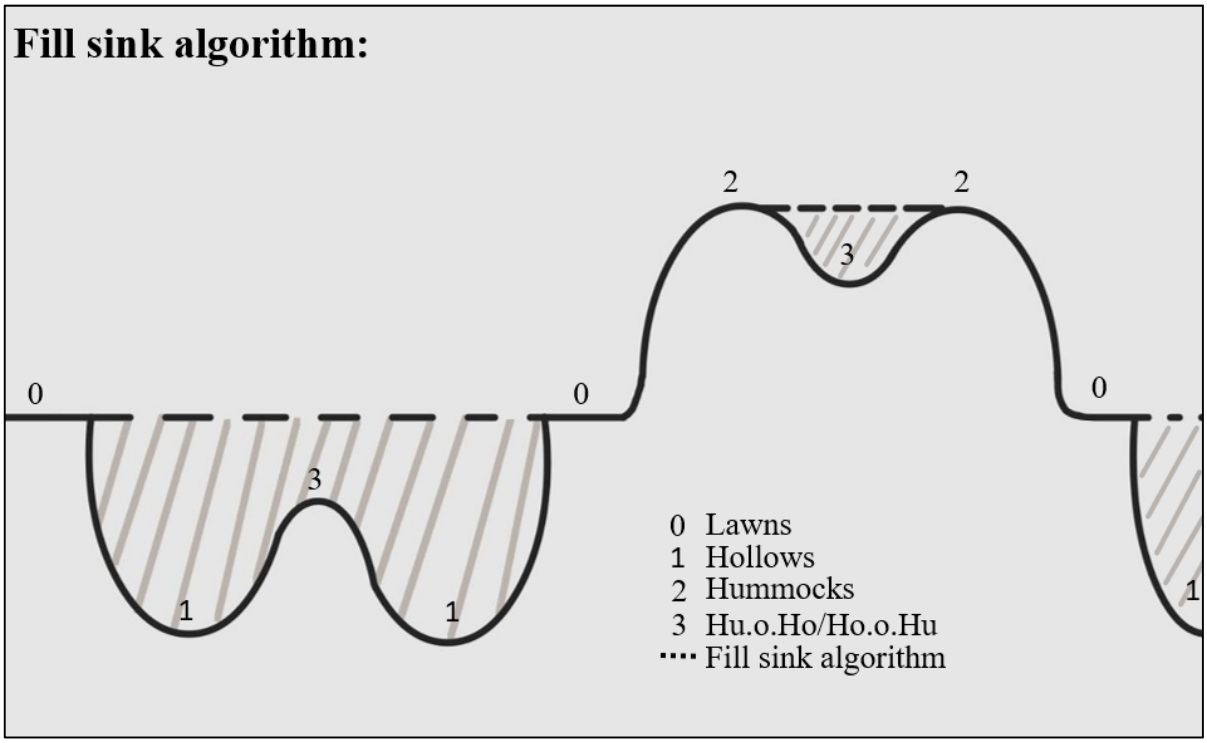

Figure 3 Graphic illustrating microtopographic classification and fill sink algorithm of the modelling approach. Hu.i.Ho. represents the subset of class 3 that are hummock- like features in hollows, and Ho.o.Hu. represents the subset of class 3 that are hollows-like depressions on hummocks.

2.3.1 Class 3 evaluation

To evaluate its relevance as a distinct class, class 3 was isolated and further split into hummock-like features in hollows (Hu.i.Ho.) and hollows-like depressions on hummocks (Ho.o.Hu.). The real height and depth values for both microforms were determined by clipping both the "subracted DEM" and the "Inverted-Subtracted DEM" (Figure 2) by each of the Hu.i.Ho. and Ho.o.Hu. layers. These absolute heights (a2, b2) and depths (a1, b1) for both sub classes are illustrated in Figure 5. After exploring the height and depth distribution of the two sub classes (see Appendix I for further details), class 3 was merged either with hummocks or hollows based on their relative height or depth (Figure 4).

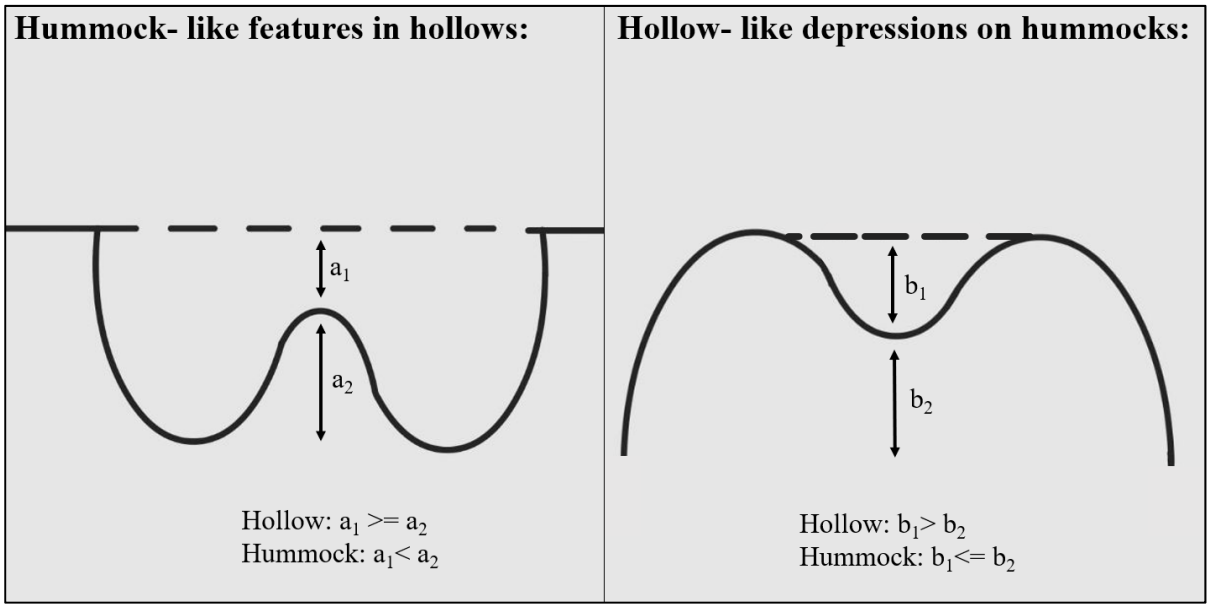

Figure 4 Height and depth values of Hu.i.Ho. (a1, a2) and Ho.o.Hu. (b1, b2) as well as spatial queries to resolve class 3.

2.3.2 Validation of the microtopography model

The microtopography results were validated at Degerö Stormyr, in a radius of 500 m around the EC tower. For almost the entire study period the studied mire sites were covered by snow making an extensive field validation impossible. Instead an image based interpretation of the UAV image blended with the DEM served as ground truth in a first step followed by a reduced one-day field validation in May. In general, the validation dataset is based on two sets of control points. The first set of control points were generated along the network of boardwalks and 2 m away to avoid the artifacts created by the boardwalk, with a 4 m spacing between points (total of 231 points). The second set of points consisted of 25 random points that served each as the center for a systematic square grid of 9 points, spaced 5 x 5 m (total of 225 points). The centers of the second set of points were constrained to at least 10 m away from the boardwalk and at least 50 m from each other.

On May 10th 2023, a field visit was carried out to validate the points along the boardwalk since the mire was still flooded and difficult to walk on for validating the other points. The visual interpretation in the field was difficult due to several lawns still flooded, making easy a confusion between the different classes.
Confusion matrices were computed in QGIS using the "Classification Layer Accuracy and Area Report (for Simple Random Sampling)" tool from the "EnMAP" plugin (Guanter et al., 2015).

The matrices allow the computation of user accuracy (UA), producer accuracy (PA) for each class, but also an overall accuracy (OA) for all classes together. The three accuracy measures

as well as omission (Om. Err.) and commission (Comm. Err.) errors were calculated as mentioned in the equations (Eq. 2-6) below (Humboldt-Universität zu Berlin, 2021).

$$OA = \frac{Number\ of\ correctly\ identified\ samples}{Number\ of\ samples} \quad \text{(Eq. 2)}$$

$$PA_c = \frac{Number\ of\ correctly\ classified\ samples\ of\ c}{Sum\ of\ samples\ with\ true\ label\ for\ c} \quad \text{(Eq. 3)}$$

$$Om.\ Err._c = 100\% - PA_c \quad \text{(Eq. 4)}$$

$$UA_c = \frac{Number\ of\ correctly\ classified\ samples\ of\ c}{Sum\ of\ samples\ classified\ as\ c} \quad \text{(Eq. 5)}$$

$$Comm.\ Err._c = 100\% - UA_c \quad \text{(Eq. 6),}$$

Equation 2-6 Where the subscript "$_c$" indicates that the metrics was computed for each class "$_c$".

Furthermore, Cohen's Kappa coefficient (Cohen, 1960) was calculated based on the confusion matrices. The Kappa coefficient evaluates how well classification performs in comparison to a random distribution. It ranges from -1 to 1 where 0 indicates that the classification is not better performing than random, and 1 indicates a perfect agreement between the different classes (Lillesand et al., 2008).

2.4 Vegetation classification

The vegetation classification of the different plant communities was performed following an object-based image analysis approach (OBIA) on the UAV images. The vegetation classification was performed using Orfeo Toolbox in QGIS (QGIS Development Team, 2023), with the workflow presented in Figure 5.

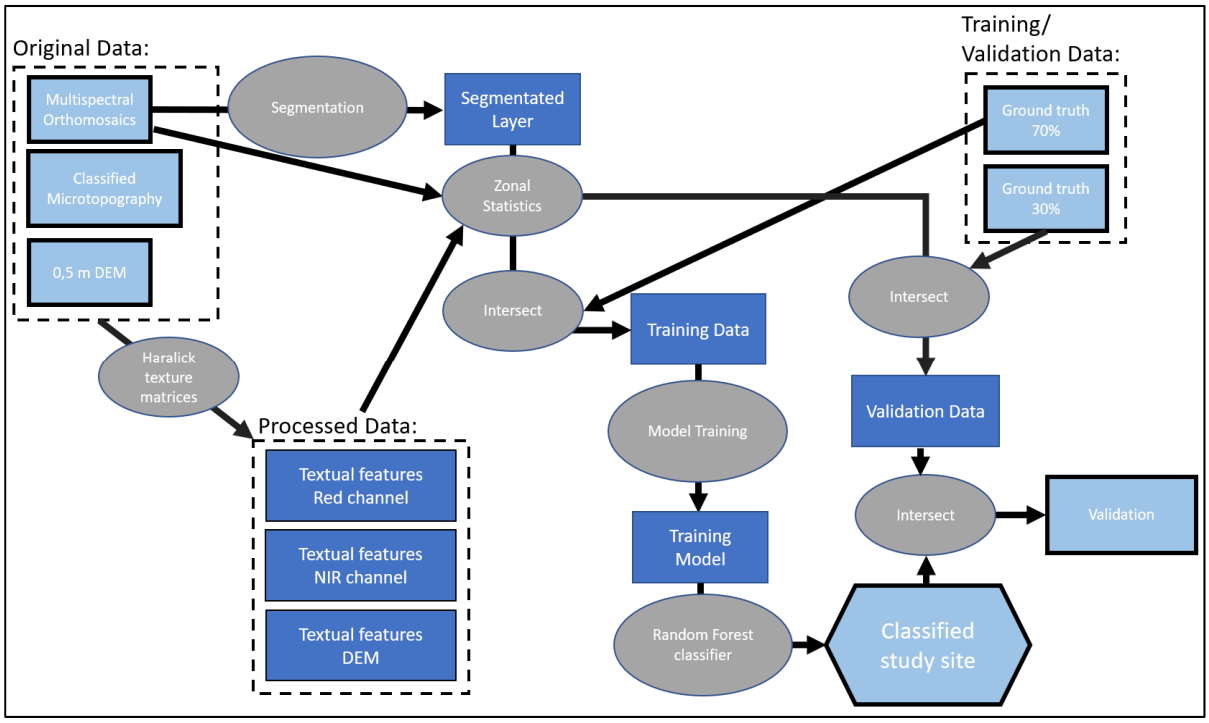

Figure 5 Object based image analysis workflow. Tools and processing steps as elliptic gray features. Resulting layers in dark blue squares. In- and output in light blue.

2.4.1 Segmentation

In OBIA approaches, image segmentation is the first step in order to create objects of similar spectral properties, which are then subsequently the entity for the classification (Martínez Prentice et al., 2021) (Figure 5). The Segmentation step was based on the multispectral orthomosaics for each site and was implemented using the "Segmentation" tool from the Orfeo Toolbox. Several segmentation algorithms exist and are based on either edge, color or texture changes for clustering groups of pixels (Mohan & Leela, 2013). In this study I used the "Mean shift" algorithm, which is a non- parametric unsupervised algorithm. Pixels were clustered and afterwards gradually shifted to the weighted mean of its local area, resulting in homogenous segments (Mohan & Leela, 2013). Mean shift is one of the most applied algorithms (Martínez Prentice et al., 2021; Michel et al., 2015) and has the following advantages:

- No initialization of segment number required,
- Possibility to tune the minimum segments size as well as the spatial and spectral range,
- Robust against outliers,

- Stable and efficient segmentation by splitting the image into tiles.

The algorithm settings such as the spatial radius, range size (spectral range) and minimum region size were adapted to the 0.03 m x 0.03 m pixel size of the UAV images. Minimum area was set to 10 Pixels meaning that the smallest segments can have a size of 90 cm^2, in order to capture the small-scale variations of vegetation composition.

2.4.2 Zonal statistics

Zonal statistics (majority and standard deviation for microtopography, mean and standard deviation for the other raster data) were computed on each several input data deemed potentially useful in the classification, with the objects resulting from the segmentation as zones (Figure 5). The input raster data for the zonal statistics were the five bands of the orthomosaics, the DEM, the microtopography classes as well as eight textural greyscale matrices for the red, near infrared bands and the DEM, respectively. The greyscale matrices are spatial dependency matrices, represent spatial differences on a chosen window size (Haralick et al.,1973).

I considered the following greyscale matrices: entropy, energy (texture uniformity), correlation (between certain pixel and it's neighborhood), inverse difference moment (measures texture homogeneity), inertia (intensity contrast between pixel and it's neighborhood), cluster shade, cluster prominence and Haralick correlation. Among the previous matrices, entropy is often considered the most meaningful textural information. Entropy is a measure of randomness or, in other words, the degree of disorder present between pixels. It is largest, when pixels represented in the matrix show high similarity and small when there is a lot of heterogeneity between pixels (Zayed & Elnemr, 2015). The greyscale matrices were computed using the "HaralickTextureExtraction" tool (Grizonnet et al., 2017). A window size of 10x 10 pixels was chosen for the Haralick analysis. Altogether, 60 variables were obtained from the zonal statistics performed on the different bands of the orthomosaic, the microtopography, the DEM and the greyscale matrices.

2.4.3 Training and validation data preparation

The ROI drawn from the vegetation inventory data covering all 7 classes included in the vegetation classification were used both for training and validation. Ground truth polygons bigger than 15 m2 were subdivided into 4 tiles to simply increase their total number. Afterwards, polygons were randomly split into 70% (training set) and 30% (validation set) per class for each study site. The training set was intersected with the segmented layer containing all zonal statistics needed for the training.

2.4.4 Random forest classification

The random forest (RF) classifier was used to classify the segmented layers into one of the seven defined classes (Table 3). The training was performed using the "TrainVectorClassifier" tool. RF is an ensemble classifier producing multiple decision trees from a randomly selected

subset of training samples. The remaining training samples are used for internal cross validation to estimate the RF performance (Belgiu & Drăgu, 2016). Two models (one including microtopography statistics and the other excluding them) were generated for each study site using the following settings for the RF model: 500 for the maximum number of decision trees, 15 for the maximum tree depth and 20 for the minimum sample size in each node. In addition, the same procedure (2 additional models) was repeated excluding the DEM based variables to explore their potential interference with the microtopography statistics. All four models were finally used as inputs for the "VectorClassifier" tool to classify all the segmented layers into the seven defined classes at all four study sites.

2.4.5 Validation

The 30% set of ground truth left out for validation was intersected with the final classification layer to obtain a shapefile containing both ground truth and predicted values for each segment. This served as ground for computing confusion matrices and an overall accuracy as well as a Kappa coefficient for all models. The accuracy metrics are presented in Tables 6 and 7, and all confusion matrices are available in the appendix (Appendix II, A-P). A Student's t-test was performed in R on all pairs of Kappa coefficient to compare statistically accuracy results with or without microtopography related statistics (R Core Team, 2023).

3. Results

The first part of the results section is dedicated to microtopographic modeling results and validation. In the second part the focus lies on vegetation classification results and the influence of microtopography and DEM based textural greyscale matrices parameters on classification accuracy.

3.1 Microtopographic feature distribution

A first visual appraisal of the two final raster layers seem to realistically reflect the microtopography variations for all four sites of this heterogenous mire complex in terms of shape and distribution. Locally more or less developed string and flark patterns indicate Aapa mire patches, that play a central role in this mire ecosystem. In Figure 6 a bigger string and flark patch close to the Degerö boardwalk can be identified. These Aapa mire areas are typically occurring on water surplus areas with water moving on a slight downslope (Rydin et al., 1999). They are surrounded by patterned and unpatternd fens with fast lawns. In other places the typical morphology of raised bog elements and hummock ridges are present in the maps (Figure 6- A, B, C, D).

The microtopographic class distribution got illustrated for 300 m buffers around the four flux towers (Figure 6- A, B, C, D). Relative occurrence (%) of all three classes got calculated from the relative proportion of class wise pixel counts for the whole mire extend (Table 4) as well as for the site buffers individually (Figure 6). In general, Lawns can be seen as the more or less dominant class ranging from 43.63 % in Degerö (Figure 6- A, E) up to 65.14 % inside the Hålmyran buffer (Figure 6- D, E), reaching 53.88 % for buffer average (Figure 6- E). On the whole Degerö/ Stortjärn extend they account for 56.59 % and on Hålmyran/ Hälsingfors for 57.71% of the area (Table 4). Looking at the relation between hummock and hollow it is striking that both structures occur in a relatively balanced ratio with an overall buffer occurrence of 22% for hollows and 24% for hummocks (Figure 6- F). On the Degerö/ Stortjärn area hummocks have a share of 22.82% and hollows of 20.59%. On the Hålmyran/ Hälsingfors extend, hummocks occur on 22.85% and hollows on 19.44% of the area (Table 4). The relative occurrence of 1:1 or a bimodal distribution is also stated in topic related literature (Graham et al., 2020; Lovitt et al., 2017; Moore et al., 2019).

Table 4 Pixel count and percentage of occurrence for microtopographic feature types along the full extends of both microtopographic layers Degerö/Stortjärn and Hålmyran/ Hälsingfors.

	Class	Pixel count	Occurrence (%)		Class	Pixel count	Occurrence (%)
Degerö/ Stortjärn	Lawns	4.996.078	56.59	**Hålmyran/ Hälsingfors**	Lawn	2.440.402	57.71
	Hollow	1.818.086	20.59		Hollow	822.237	19.44
	Hummock	2.014.518	22.82		Hummock	966.353	22.85
	Sum	8.828.682	100.00		Sum	4.228.992	100.00

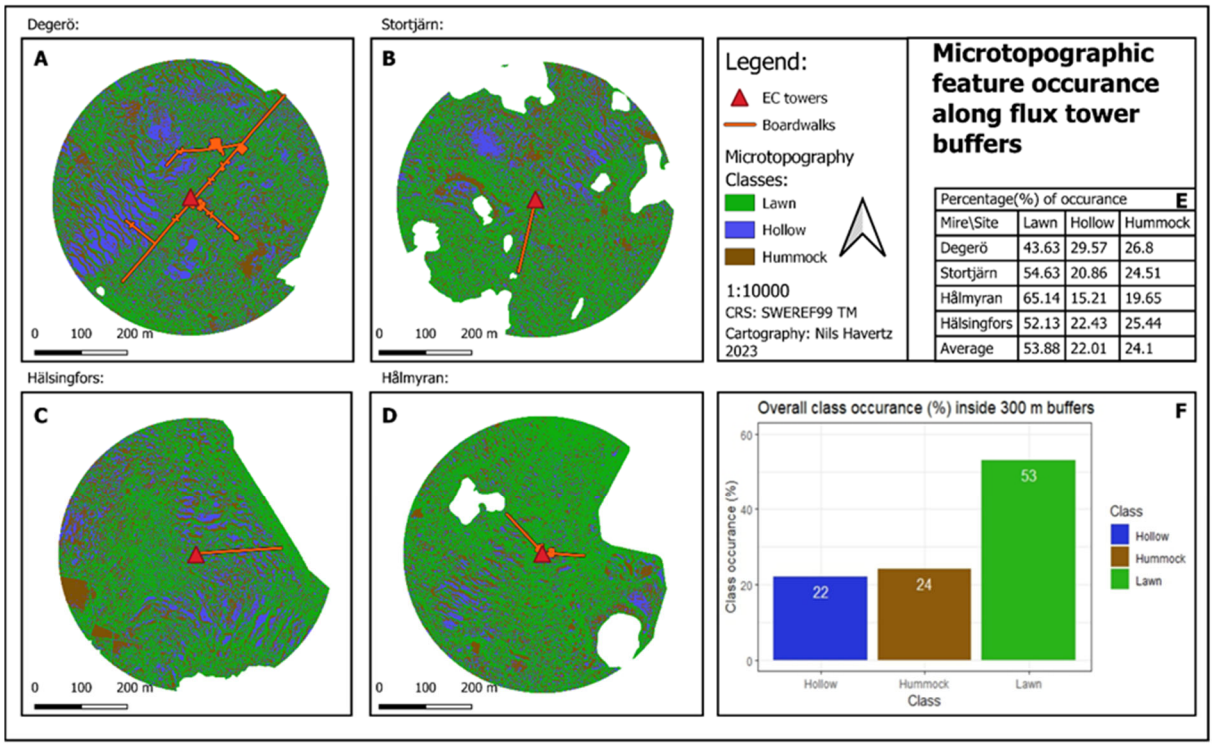

Figure 6 Mapping results of microtopographic feature occurrence along the flux towers (A-D). Table (E) showing feature occurrence site wise and as an average. Bar chart (F) representing the overall class occurrence inside the 300 m buffers based on the sum of all.

3.2 Validation results

3.2.1 Image interpretation validation

The accuracy scores and the kappa coefficient resulting from the image interpretation validation process are presented in three accuracy matrices separately for boardwalk and the buffer points as well as for all sample points together, in Table 5. The overall accuracy (OA) does not differ much between the three matrices and is slightly above 0.67 (67%). Mire patches along the Degerö boardwalk are characterized by a high lawn percentage and the whole area shows strong charachteristics of unpatterned fens also displayed in dominant lawn occurrence resulting in an unequal class distribution (Figure 6).

The cross evaluation of columns and rows of the confusion matrices reveals misleading results mainly appear between lawns and hummocks as well as lawns and hollows. In the hummock and hollow columns for all three matrices the number of wrongly classified points as lawns are much higher than for the other corresponding feature (hummock or hollow). On the other hand the confusion in the lawn columns seems more or less equally allocated between hollows and hummocks (Table 5).

Comparing the individual class accuracies, it is striking that hummocks show a quite low producer accuracy (PA) between 0.5- 0.57 in all three tables, whereas the user accuracies (UA) varies more between 0.81 inside the buffer and 0.60 along the boardwalk. Hollows UA result range is quite narrow 0.71-0.73, on a contrary there is a gap between 0.61 for boardwalk and 0.73 for buffer producer accuracy (Table 5). For lawns the PA between 0.73-0.79 reveal better results than the lower UA between 0.56-0.68 (Table 5). This indicates an over classification of lawns reflected in a higher PA and a lower UA compared to hollows and hummocks. Furthermore, misclassified hummocks and hollows as lawns lower their producer accuracy scores.
The kappa coefficient of 0.50 for the summarized sample points, 0.51 for the boardwalk points and 0.47 can be interpreted a little bit more pessimistic in relative to the overall accuracy results and emphasizes the divergent results between PA and UA (Table 5).

Table 5 Accuracy assessment results from the image based interpretation based on the microtopography sampling points and presented by confusion matrices. Buffer points and boardwalk points analyzed separately and together (Sum points).

Sum points		Reference					
Predicted		Lawn	Hollow	Hummock	Total	User's accuracy	Comm. error
	Lawn	143	37	48	228	0.63	0.37
	Hollow	23	91	13	127	0.72	0.28
	Hummock	20	8	73	101	0.72	0.28
	Total	186	136	134	456		
	Prod. accuracy	0.77	0.67	0.54		Kappa coefficient:	**0.50**
	Omm. Error	0.23	0.33	0.46		Overall accuracy:	**0.67**
Boardwalk points		**Reference**					
Predicted		Lawn	Hollow	Hummock	Total	User's accuracy	Comm. error
	Lawn	88	21	21	130	0.68	0.32
	Hollow	12	43	4	59	0.73	0.27
	Hummock	11	6	25	42	0.60	0.40
	Total	111	70	50	231		
	Prod. accuracy	0.79	0.61	0.5		Kappa coefficient:	**0.51**
	Omm. Error	0.21	0.39	0.5		Overall accuracy:	**0.68**
Buffer points		**Reference**					
Predicted		Lawn	Hollow	Hummock	Total	User's accuracy	Comm. error
	Lawn	55	16	27	98	0.56	0.44
	Hollow	11	48	9	68	0.71	0.29
	Hummock	9	2	48	59	0.81	0.19
	Total	75	66	84	225		
	Prod. accuracy	0.73	0.73	0.57		Kappa coefficient:	**0.47**
	Omm. Error	0.27	0.27	0.43		Overall accuracy:	**0.67**

3.2.2 Field validation

The field validation comes to a similar overall accuracy of 0.67 (67%) (Table 6). Apart from that, class wise user and producer accuracy as well as kappa coefficient differ distinctly from image interpretation validation. In general, image, field and model interpretation of the validation points show divergent classification interpretation between each other indicating the difficulty of threshold setting considering moving water table and vegetation cycles. A column and row cross evaluation designates again a main confusion between lawns and the corresponding hummock or hollow features, whereas the differentiation of hollows and hummocks seems to be clear. Producer accuracies for all three classes are ranging from 0.66 for hollows 0.68 for hummocks. User accuracies vary greater from each other. Hummock UA of 0.38 and hollow

UA of 0.49 are quite low, whereas the UA for lawns is about 0.84. Pa and UA values draw an almost opposite picture to the image interpretation classification.

The misclassification of lawns that should be hummocks or hollows is relatively low whereas a higher proportion of hummock and hollow classified features are referenced in the field as lawns. The kappa coefficient of 0.38 also decreased compared to the image interpretation accuracy results and is generally affected by the unequal class occurrences and divergent PA and UA (Table 6).

Table 6 Accuracy assessment results from the field assessment based on the microtopography buffer sampling points and presented by confusion matrices.

Field validation		**Reference**					
Predicted		**Lawn**	**Hollow**	**Hummock**	**Total**	**User's accuracy**	**Comm. Error**
	Lawn	97	13	5	115	0.84	0.16
	Hollow	29	29	1	59	0.49	0.51
	Hummock	19	2	13	34	0.38	0.62
	Total	145	44	19	208		
	Prod. Accuracy	0.67	0.66	0.68		**Kappa coefficient:**	**0.38**
	Omm. Error	0.33	0.34	0.32		**Overall accuracy:**	**0.67**

3.3 Vegetation classification results

The mapping results for the vegetation classification including microtopography as an input variable are presented for the 300 m buffers around the flux towers in Figure 7- A, B, C, D. In addition, class occurrences for the buffers of each site as well as the overall class occurrence of all sites together are shown in Figure 7- E and Figure 7- F. For Stortjärn (Figure 7- B), Hälsingfors (Figure 7- C) and Hålmyran (Figure 7- D) the buffer radius exceeds the extent of the UAV images resulting in non-circular subsets. Here is a recall of the classes considered in this classification, as described in Table 3:

- Class 1: Lawns dominated by short sedges and Sphagna
- Class 2: Hollows/Carpets dominated by short sedges and Sphagnum subg. Cuspidata
- Class 3: Hollows/Mud or loose bottoms, tall sedge fens
- Class 4: Hummocks and sparely treed mires
- Class 5: Mire forests including high hummocks
- Class 6: Broadwalks and artificial structures
- Class 7: Open waters

The heterogeneity in class occurrence across the study sites reflects the diversity of this mixed boreal mire. Class 6 and 7 cover only a very marginal proportion on all sites. Inside the Degerö and Stortjärn 300 m buffers, mire forests including high hummocks (Class 5), is the dominating

plant community form accounting for 40.99 % in Degerö (Figure 7- A, E) and 49.37% on the Stortjärn site (Figure 7- B, E). The class mainly occurs in larger clusters at higher elevated areas at the edges of the buffers (Figure 7). Class 4 appears on about 23% of both sites (Degerö and Stortjärn) followed by class 1 with 17.07% in Degerö and 23.09% inside Stortjärn buffer. Class 2 and 3 representing vegetation groupings associated with hollows and lower level lawns share 18.33% of the buffer at Degerö and only 3.86% at the Stortjärn site. For Hålmyran and Hälsingfors, class 4 is the most abundant one, making 41.37% of the total occurrence at Hålmyran (Figure 7- D, E) and 32.05% at Hälsingfors (Figure 7- C, E). Class 5 is the second largest class at Hålmyran with 26.50%, whereas it occurred the least at Hälsingfors on 8.83% of the buffer. For both study sites, class 1 covers more than 20% of the buffer. Hälsingfors has the highest values for the hollow-lower level lawn associated vegetation with 20.64% for class 2 and 11.89% for class 3 (Figure 7- C, E). On the other hand, both class 2 and 3 share only 6.08% of the buffer at Hålmyran (Figure 7- D, E). The overall class occurrence reveals, that class 4 with 29.15% and 5 with 31.07% make the dominant vegetation cover around the flux towers, followed by class 1 with 20.25% and class 2 with 12.71% (Figure 7- F). Class 3 only has a minor share of 5.83%.

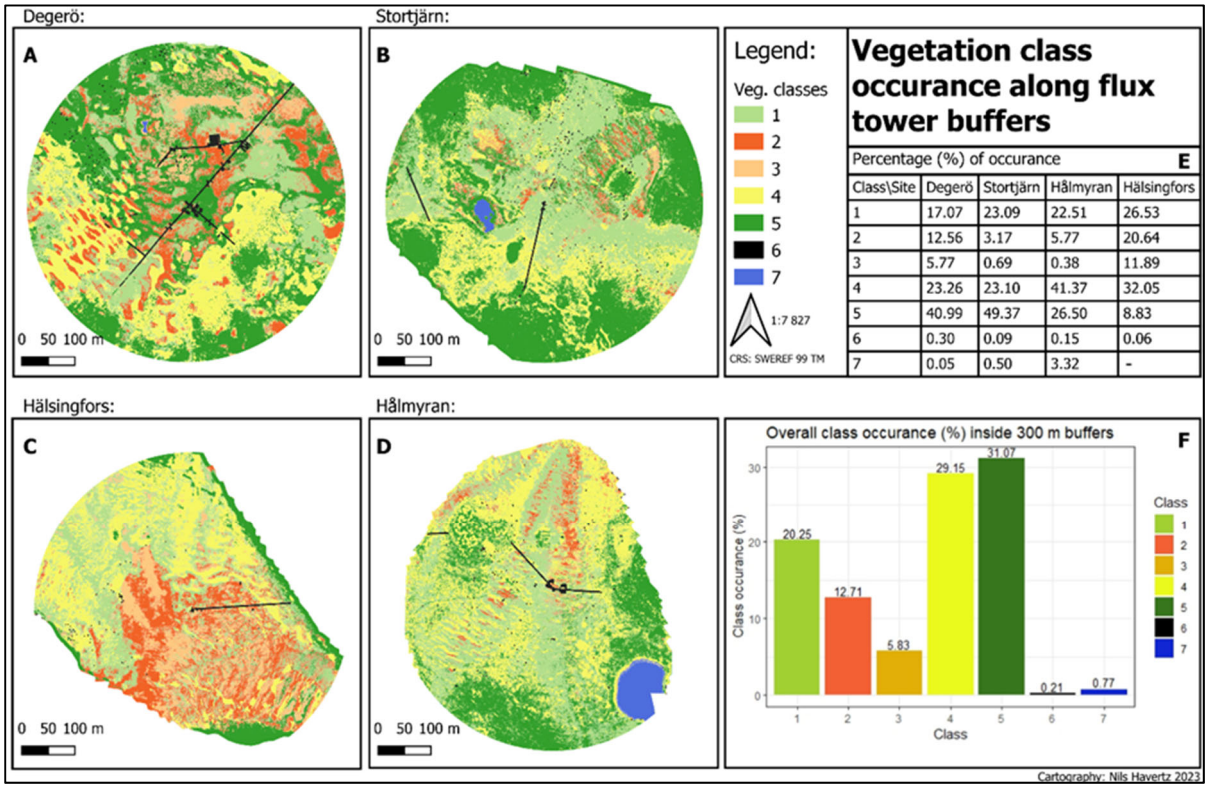

Figure 7 Mapping results of the vegetation classification including all input variables, inside 300 buffers along the flux towers. Table displaying the class occurrence site wise. Bar graph illustrating the total class occurrence for all sites.

3.4 The influence of microtopography on classification accuracy

Overall accuracy and Kappa coefficient for all four sites are presented in Table 7 including both, classification with and without microtopography. The corresponding confusion matrices can be found in the appendix (Appendix II A-P). The average overall accurracy for both classification procedures was about 85%, with an average Kappa coefficient of 0.78, suggesting a good agreement between the classifications and the truth. Some artifacts in the classification can be seen where class 6 appeared as dots in some parts of the buffers where there is no boardwalk, likely following artifacts in the orthomosaics (Figure 7).

Table 7 Accuracy results for vegetation classification with and without microtopography as an input variable and DEM texture measures as an obligatory input.

Site	Overall accuracy		Kappa coefficient	
	With microtop.	Without microtop.	With microtop.	Without microtop.
Degerö	0.90	0.89	0.83	0.83
Stortjärn	0.84	0.84	0.72	0.72
Hålmyran	0.86	0.85	0.80	0.78
Hälsingfors	0.84	0.83	0.80	0.78
Average	**0.86**	**0.85**	**0.79**	**0.78**

The highest overall accuracy and Kappa coefficient were obtained at Degerö including microtopography, with an overall accuracy value of 0.90 and corresponding Kappa coefficient of 0.83. Lowest Kappa coefficient of 0.72 can be found at Stortjärn with microtopography whereas the lowest overall accuracy of 0.83 is recorded at Hälsingfors without microtopography. Altogether, T-test result for the Kappa coefficients gave a p-value of 0.09, indicating no significant effect of the inclusion of microtopography in the classification, at 5% significance level.

When excluding DEM extracted Haralick texture metrics from the inputs for the classification, the obtained accuracy metrics are lower overall (Table 8) compared to Table 7. However, there is more effect of microtography as reflected by the higher overall accuracy and Kappa coefficient when including microtopography as an input for the classification, even though the T-test showed a barely significant difference (p-value = 0.04977).

Table 8 Accuracy results for vegetation classification with and without microtopography as an input variable excluding DEM texture measures as an obligatory input.

Site	Overall accuracy		Kappa coefficient	
	With microtop.	**Without microtop.**	**With microtop.**	**Without microtop.**
Degerö	0.83	0.81	0.72	0.68
Stortjärn	0.78	0.77	0.62	0.61
Hålmyran	0.83	0.82	0.75	0.73
Hälsingfors	0.78	0.74	0.71	0.67
Average	**0.80**	**0.78**	**0.70**	**0.67**

4. Discussion

4.1 Overall performance of the new microtopography modelling approach

Before discussing advantages and limitations of the applied modelling approach it should be stated, that all microform classification schemes mentioned in Table 1 have their specific purpose and are suitable in different ways. In fact, each method targets explicitly defined objectives, and a comparison between studies should be made in awareness of each method's specificity (Graham et al., 2020). The objectives of the new approach are the simplification of an otherwise very complex microtopography classification as well as the reduction to a single input, a DEM, while achieving more than the usual binary class scheme (hummock-hollow) by also identifying lawns. Computational time and reproducibility are optimized through an easy-to-use python script and graphic models for QGIS available under the GitHub link stated in section 2.3.

The obtained results suggest that a resolution of 50 cm input data is suitable for mapping larger extends, here tested on ~300 ha in the mire sites of the Kulbäcksliden Research Infrastructure. Several previous studies have shown that the lowest resolution for characterizing microtopographic parameters and their variance is about 0.5 m (Graham et al., 2020; Moore et al., 2019). The generally balanced proportion of hummocks and hollow (Result section 3.1, Figure 6 and Table 4) is in agreement with previous findings suggesting a 1:1 occurrence of the two classes in general (Graham et al., 2020; Lovitt et al., 2018). The inclusion of a third class did not alter the relative proportion between hummocks and hollows (as observed in the binary classification), but has instead simply reduced their occurrence equally in favor of the lawns intermediary class.

Microtopography is not a discrete element in mires. Instead, they occur as a continuum on the mire surface, making distinctions difficult to make in modelling studies. In the present study, the class 3 here referred to as hummocky structures along hollows and small depressions on hummocks seems interesting since it could be reflecting different biogeochemical processes from the surrounding hummock or hollow. The here stated approach gives the option to either merge or keep that intermediate class, depending on the aim of the classification. In addition,

field observation and validation could give more information about the relevance and effects of those structures.

The sink filling algorithm has proved applicability on a 50 cm ground resolution DEM. A first brief performance check of the modelling approach on a finer DEM with spatial resolution of 0.3 x 0.3 m revealed some problems concerning the workflow, with a more fragmented microtopography, and more class 3 (classified both as hollow and hummock) to be merged with either the hollow or hummock class, over the whole study area. Increasing the threshold for deciding what should be a hummock or a hollow instead of any filled pixel (threshold = 0) could allow the use of higher resolution DEM while achieving an accurate classification. All in all, the new method shows promising potential to become another option for quantitative modeling of microtopography and fills the gaps of simplicity concerning input data and computation time and effort as well as straight forward large scale mapping results, compared to other studies. However, the validation results also revealed errors that need to be corrected by optimization steps and evaluated again for a final publishment.

4.2 Microtopography validation and error assessment

Even though the accuracy results overall do not indicate a fully accurate model they reveal promising trends in clear distinct relief patches and optimization targets at the boundary of lawns to hummock and hollow features. It should be noted that the validation is limited in many respects and its representativeness is therefore questionable. Both the image interpretation as well as the infield reference classification is inherently subjective due to generally small elevation differences as well as the edge complexity of microforms (Stovall et al., 2019).

Added to this are the monthly fluctuating vegetative and hydrological conditions, which ultimately lead to biased classification results seen in between image, in field and model classification (Moore et al., 2019). The timing of the field visit which occurred right after snow melt made it difficult to distinguish lower level lawns from hollows, and upper level lawns from hummocks in some cases due to the very high water table level. Moreover, the unequal class distribution along the Degerö Stormyr boardwalk where field validation occurred can be considered a limiting factor for a more realistic field validation since this influenced the considered accuracy metrics. Another factor that has become apparent in the field was the elevated altitude of the boardwalk in the DEM in some parts, acting as a hummock and therefore affecting the actual microtopography in its neighborhood. Despite accounting for this fact when choosing the validation points 2 m away from the boardwalk, it was apparent that this distance did not suffice in some cases. Instead of using systematic and cluster sampling, stratified sampling methods are recommendable for more reliable validation by guarantying a more balanced class occurrence (Köhl et al., 2006).

The factors of uncertainty are reflected in the divergent class attribution of the image based, in-field and model classification. Both validations clearly indicate that the confusion mostly refers to the edges of intermediate lawn stages to hummocks and hollows (Table 5, 6). From the field validation confusion matrix, it appears that several hummocks and hollows should instead be classified as lawns, which is also displayed in a higher lawn PA and a low lawn UA (Table 6).

Overall, most cases of mismatch occurred in shallow-large sinks (lower level lawns) or extended slightly elevated areas, not high enough to be a hummock, but acting as a depression in the inverted DEM (upper level lawns). There is a tendency for overestimation of hollows and hummocks on slight depressions and slightly elevated areas, respectively, as indicated in Table 6. A simple introduction of an intermediate class as suggested by Lovitt et al. (2017) and Stovall et al. (2019) itself does not solve the uncertainties without meaningful thresholds.

The errors caused by the overestimation of hummock and hollows on the edge of the intermediate lawn stage could likely be reduced by finding new appropriate height and depth thresholds in the reclassification step for the "Subtracted DEM" and "Inverted- Substracted-DEM" (Figure 2). The classification threshold of 0.00001 m used in the analysis here seem to be way too low. A quick test setting a threshold of 3 cm fill depth (0.03 m) for the identification of hollows and hummocks increased the overall accuracy to 0.82 computed from the field validation data. This is a promising improvement that could be explored further. In fact, lawns tend to range in their elevation a bit more than expected before. Another alternative could be the introduction of two more classes to improve the specification of the intermediate. In literature low level lawns or carpets and high level lawns are commonly used for microtopography description and applicable by diversifying the reclassification step (Korpela et al., 2020; Rydin et al., 1999).

When aiming for mapping raster data on finer resolutions, more complex or broader classification approaches are purposeful alternative as long as the here stated approach does not give accurate results at such resolutions. For instance, Korpela et al. (2020) computed seven features for classifying microforms from a LiDAR DEM, including: Standard deviation of 0.3 m window surface roughness and slope, range of slope values, hummock index looking at minimum elevation, depression index to find small-scale variations, flatness index consists of smallest sum of elevation, distance to closest hummock border, texture feature contrast. They also emphasized the usefulness of combining spectral information generated by LiDAR data with passive sensor information from multispectral UAV images for improving microform classification results. Kalacska et al., (2021) stated the overall higher point density of SfM UAV compared to airborne based LiDAR data that could be another factor supporting the combination of both platforms when aiming for highest accurate modelling results.

4.3 Microtopography model application prospect

It is important to notice that microtopography is not a phenomenon only occurring in northern peatlands. In fact, they play a central role on different scales in most wetland types such as salt marches and forest wetlands (Craft, 2016). Most studies until now have focused on northern and especially boreal peatlands where we can find the most distinct microtopographic patterns (Joosten & Clarke, 2002), although some studies can be found on other wetland types (Minick et al., 2021; Stovall et al., 2019). Temperate fens and bogs found in northern Germany and around the baltic states have been less targeted when it comes to microtopography modelling in a more quantitative sense (Couwenberg & Joosten, 2005). Microforms in german literature referred to as "Kleinformen" (Joosten & Clarke, 2002) show distinct morphology from boreal feature types, originating from glacial processes (Lindner-Effland, 2002). However, independently of the origin, microforms affect small-scale variations in nutrient and water supply in these ecosystems (Szporak-Wasilewska et al., 2021) and therefore should be considered in research on a global scale.

Wetland and peatlands are particularly threatened nowadays in multiple ways. Anthropogenic use usually leads to the draining of ecosystems already stressed by climate change. Microtopography patterns do not only form but also stabilize the entire ecosystem and are able to reduce water outflow (Craft, 2016). When it comes to peatland restoration the creation of microtopography helps developing moister habitats especially in hollows, producing a more favorable situation for Sphagnum to reestablish (Campeau et al., 2004).

The aspects mentioned here as well as in section 1.4 clearly underline the importance of diverse microtopographic modelling approaches and the need for continuous topic related research as well as constant improvement along the latest technological advances in RS. The here tested approach opens an opportunity for a broad use in environmental applications through its low requirements and fast computational time.

4.4 Segmentation settings

In OBIA, segmentation settings have a major impact on classification results and can be considered as a complex task due to overall low spectral contrast of peatland plant communities. It is also important to adapt segmentation settings to class area, spatial and spectral ranges (Huiping et al., 2003). Segmentation settings were based on trial and error using a test area before final segmentation. Segment size and the spectral range were based on the estimated minimum spatial size and variability of the vegetation groups on the ground and the spectral resolution of each band. An alternative approach to the subjective approach adopted in this study is the application of a genetic algorithm (GA) to realize an evolutionary process of parameter settings in order find optimal solutions for segmentation (Martínez Prentice et al., 2021). The here used segmentation algorithm performed well, but the segment size of 90 cm^2

show slight tendencies to be too small. Applying a GA in advance could optimize the segmentation process.

4.5 Vegetation classification performance and the influence of microtopography

The best random forest performances were obtained when using all 62 possible input parameters. The different band statistics and Haralick texture metrics seemed to provide enough information for the vegetation classification, and the classification was only improved very little by the inclusion of microtopography, and even less when also including DEM-derived Haralick texture metrics. The marginal effect of microtopography and elevation data on the classification results in this study does not reflect the well-known dependence of plant species distribution and biogeochemical processes on microtopography (Couwenberg & Joosten, 2005; Nungesser, 2003; Pouliot et al., 2011). In addition, it should be noted that the vegetation classes are relatively wide and, as the mapping results show, their classification is usually on a larger spatial level than the variation of the microforms. A comparison of the mapping results can be found for a small extend along the Degerö boardwalk in the appendix (Appendix III). The overestimation of hummocks and hollows (Discussion section 4.2) likely lowered the effect of microtopography on vegetation classification by wrongly fragmenting vast lawn patches into more heterogenous small scale variations of all three classes. The match between larger single microform features and suitable vegetation classification results support this assumption.

A misclassified class 5 extend can be observed along the Degerö boardwalk, which should be either class 1 or 2. Considering this the generation of more training features either in the field or based on the drone image are recommendable to solve these errors.

A suggestable option to optimize classification could be to include vegetation indices to the classification, with their ability to enhance differences between plant communities (Martínez Prentice et al., 2021). Greenness indices, leaf pigment indices and photosynthetic indices were proved to improve classification accuracies on alkaline fens in Poland (Szporak-Wasilewska et al., 2021). Moreover, laser scanning topographical products are also useful in vegetation classification, besides hyperspectral data for modeling topographic differences influencing plant cover through water and nutrient supply (Szporak-Wasilewska et al., 2021; Korpela et al., 2020). This is in agreement with the increased accuracy, though very small, observed in the present study when incorporating microtopography classes into vegetation classification. Considering the here stated solutions for solving the weak points found after validation as well as using the microtopographic model with adjusted height thresholds as a input, should increase the accuracy of the otherwise solid performed vegetation classification.

5. Conclusion

In this study, a simple approach for modelling and classifying microtopography along a large mire extent was evaluated. Furthermore, the effect of microtopography inclusion as an input for vegetation classification got analyzed. The results of the microtopography modelling approach indicated promising applicability on 50 cm ground resolution DEM, but raised the need to optimize the threshold for a more accurate identification of hummocks and hollows. Limitations for finer resolutions are detected and potential areas of improvement were discussed. Overall, the new approach has the potential to fill the gap of simplicity and straight forward microform mapping, lacking in other established methods mentioned previously.

The highest accuracy results for vegetation classification where obtained using all available input parameters including microtopography and DEM based metrics, even though, accounting for microtopography only resulted in a minor improvement of the overall accuracy with regards to the fine resolution spectral data of the UAV images.
The main learning outcome is, that there is no one single prefect solution for generally achieve optimal results in remote sensing. The key is more in choosing the most suitable approach for a specific application.

From the applied workflow, the validation results and considerations mentioned in the discussion, the following recommendations for optimizing the workflow and applicability of the new microtopographic modeling approach and to improve the vegetation classification accuracy can be made:

- Gaining deeper knowledge on where the computational limits of the Fill sink algorithm by Wang and Lui are and try to optimize the workflow for finer DEM resolutions.
- Examining appropriate height thresholds for distinguishing hummocks and hollows from lawns.
- Including an upper and lower lawn subclass to the microtopography modeling workflow to optimize the intermediate transition zone between hollow and hummock features.
- Using spectral information provided by multispectral drone imagery to further analyze microtopography feature determination by combining and comparing the DEM based approach applied in this study with a random forest classifier to use the strength and minimize disadvantages of both methods.

- Improving the accuracy of vegetation classification by applying GA for segmentation, generating spectral vegetation indices and the optimized microtopographic modelling workflow.

Acknowledgements

A major thanks to Koffi Dodji Noumonvi who came up with this interesting new microtopographic model idea and helped me out at any time during my thesis project. Moreover, I am also grateful to Prof. Matthias Peichl and Jonas Bohlin for helping me organizing my stay at SLU Umeå and for the useful advices during my thesis project. Finally, I would like to thank Prof. Dr. Sebastian van der Linden for taking over the role as my Supervisor in Greifswald and for the suggestions concerning the vegetation analysis part.

References

Baird, A. J., Morris, P. J., & Belye, L. R. (2012). The DigiBog peatland development model 1: rationale, conceptual model, and hydrological basis. *Ecohydrology* , *5*, pp. 242–255. doi: https://doi.org/10.1002/eco.2

Balestrieri, E., Daponte, P., De Vito, L., & Lamonaca, F. (2021). Sensors and measurements for unmanned systems: An overview. *Sensors*, *21 (4)*, pp. 1–27. doi: https://doi.org/10.3390/s21041518

Belgiu, M., & Drăgu, L. (2016). Random forest in remote sensing: A review of applications and future directions. *ISPRS Journal of Photogrammetry and Remote Sensing*,*114*, pp. 24–31. doi: https://doi.org/10.1016/j.isprsjprs.2016.01.011

Beyer, F., Jurasinski, G., Couwenberg, J., & Grenzdörffer, G. (2019). Multisensor data to derive peatland vegetation communities using a fixed-wing unmanned aerial vehicle. *International Journal of Remote Sensing*, *40(24)*, pp. 9103–9125. doi: https://doi.org/10.1080/01431161.2019.1580825

Brubaker, K. M., Myers, W. L., Drohan, P. J., Miller, D. A., & Boyer, E. W. (2013). The Use of LiDAR Terrain Data in Characterizing Surface Roughness and Microtopography. *Applied and Environmental Soil Science, 2013*, pp. 13. doi: 10.1155/2013/891534

Caldwell, M., Heldmaier, U. G., Jackson, G. R., Lange, U. O., Mooney, G. H., & Schulze, U. (2006). Boreal peatland ecosystems. *Ecological Studies* ,*188*. *Springer, Berlin and Heidelberg*

Campeau, S., Rochefort, L., & Price, J. S. (2004). On the use of shallow basins to restore cutover peatlands: Plant establishment. *Restoration Ecology*, *12*(4), pp. 471–482. doi: https://doi.org/10.1111/j.1061-2971.2004.00302.x

Cohen, J. (1960). A Coefficient of Agreement for Nominal Scales. *Educational and Psychological Measurement*, *20*(1), pp. 37–46. doi: https://doi.org/10.1177/001316446002000104

Couwenberg, J., & Joosten, H. (2005). Self-organization in raised bog patterning: The origin of microtope zonation and mesotope diversity. *Journal of Ecology*, *93*(6), pp. 1238–1248. doi: https://doi.org/10.1111/j.1365-2745.2005.01035.x

Craft, C. (2016). Peatlands. In *Creating and Restoring Wetlands*, pp. 161–192. doi: https://doi.org/10.1016/b978-0-12-407232-9.00007-5

Dodji Noumonvi, K., Ågren, A. M., Ratcliffe, J. L., Öquist, M. G., Ericson, L., Hei, C., Tong, M., Järveoja, J., Zhu, W., Osterwalder, S., Peng, H., Erefur, C., Bishop, K., Laudon, H., Nilsson, M. B., & Peichl, M. (2023). The Kulbäcksliden Research Infrastructure: a unique setting for northern peatland studies. *Frontiers in Earth Science*, *11*. doi: 10.3389/feart.2023.1194749

Ericson, L., Nilsson, M., & Noumonvi, K. D. (2021). Vegetation inventory at the Kulbäcksliden Research Infrastructure mire sites 2018 and 2021. In *Figshare*. doi: https://doi.org/10.6084/m9.figshare.22826279

Eurola, S., & Virtanen, R. (1991). Key to the vegetation of the northern Fennoscandian fjelds. *University of Helsinki*

Graham, J. D., Glenn, N. F., Spaete, L. P., & Hanson, P. J. (2020). Characterizing Peatland Microtopography Using Gradient and Microform-Based Approaches. *Ecosystems*, *23*(7), pp.1464–1480. doi: https://doi.org/10.1007/s10021-020-00481-z

Graham, J.D., Ricciuto, D. M., Ricciuto, D. M., & Hanson, P. J. (2022): Incorporating Microtopography in a Land Surface Model and Quantifying the Effect on the Carbon Cycle. *Journal of Advances in Modeling Earth Systems, 14 (2)*. doi: 10.1029/2021MS002721

Grizonnet, M., Michel, J., Poughon, V., Inglada, J., Savinaud, M., & Cresson, R. (2017). Orfeo ToolBox: open source processing of remote sensing images. *Open Geospatial Data, Software and Standards*, *2*(1). doi: https://doi.org/10.1186/s40965-017-0031-6

Haralick, R. M., Shanmugan, K., & Dinstein, I. (1973). Textural Features for Image Classification. *Transactions on Systems, Man and Cybernetics*, *SMC-3, 6*, pp. 610–621. doi: https://doi.org/10.1109/TSMC.1973.4309314

Harris, L. I., Roulet, N. T., & Moore, T. R. (2020). Mechanisms for the Development of Microform Patterns in Peatlands of the Hudson Bay Lowland. *Ecosystems*, *23*(4), pp. 741–767. doi: https://doi.org/10.1007/s10021-019-00436-z

Huiping, H., Bingfang, W., & Jinlong, F. (2003). Analysis to the Relationship of Classification Accuracy, Segmentation Scale, Image Resolution. *IEEE International Geoscience and Remote Sensing* Symposium, 6, pp. 3671–3673. doi: https://doi.org/10.1109/IGARSS.2003.1295233

Ivanov, K. E. (1981). Water Movement in Mirelands. *Academic Press, London*

Joosten, H., & Clarke, D. (2002). Wise use of mires and peatlands. *International Mire Conservation Group and International Peat Society,Totnes and Devon*

Kalacska, M., Arroyo-Mora, J. P., & Lucanus, O. (2021). Comparing Uas Lidar and structure-from-motion photogrammetry for peatland mapping and virtual reality (Vr) visualization. *Drones*, *5*(2). doi: https://doi.org/10.3390/drones5020036

Köhl, M., Magnussen, S., & Marchetti, M. (2006). *Sampling methods, remote sensing and GIS multiresource forest inventory*. *Springer, Berlin and Heidelberg*

Korpela, I., Haapanen, R., Korrensalo, A., Tuittila, E. S., & Vesala, T. (2020). Fine-resolution mapping of microforms of a boreal bog using aerial images and waveform-recording LiDAR. *Mires and Peat*, *26*. doi: https://doi.org/10.19189/MaP.2018.OMB.388

Laitinen, J., Rehell, S., & Huttunen, A. (2005). Vegetation-related hydrotopographic and hydrologic classification for aapa mires (Hirvisuo, Finland). *Ann. Bot. Fennici*, *42*, pp. 107–121

Lillesand, T. M. , Kiefer R. W. , & Chipman J. (2015). Remote sensing and Image interpretation. Eds., 6(7). *Wiley*

Lindner-Effland, M. (2002). Vegetation und Stratigraphie von Sphagnum Mooren in der Jungmoräne Schleswig- Holsteins, Mecklenburg- Vorpommerns und Südjütland. *Dissertation. University of Kiel*

Lovitt, J., Rahman, M. M., & McDermid, G. J. (2017). Assessing the value of UAV photogrammetry for characterizing terrain in complex peatlands. *Remote Sensing*, *9*(7). doi: https://doi.org/10.3390/rs9070715

Mäkilä, M., Säävuori, H., Grundström, A., & Suomi, T. (2018). Sphagnum decay patterns and bog microtopography in south-eastern Finland. *Mires and Peat*, *21*. doi: https://doi.org/10.19189/MaP.2017.OMB.283

Martínez Prentice, R., Villoslada Peciña, M., Ward, R. D., Bergamo, T. F., Joyce, C. B., & Sepp, K. (2021). Machine learning classification and accuracy assessment from high-resolution images of coastal wetlands. *Remote Sensing*, *13*(18). doi: https://doi.org/10.3390/rs13183669

Michel, J., Youssefi, D., & Grizonnet, M. (2015). Stable mean-shift algorithm and its application to the segmentation of arbitrarily large remote sensing images. *IEEE Transactions on Geoscience and Remote Sensing*, *53*(2), pp. 952–964. doi: https://doi.org/10.1109/TGRS.2014.2330857

Minick, K. J., Mitra, B., Li, X., Fischer, M., Aguilos, M., Prajapati, P., Noormets, A., & King, J. S. (2021). Wetland microtopography alters response of potential net CO2 and CH4 production to temperature and moisture: Evidence from a laboratory experiment. *Geoderma*, *402*. doi: https://doi.org/10.1016/j.geoderma.2021.115367

Mohan, S. S., & Leela, S. (2013). Importance of Mean Shift in Remote Sensing Segmentation. *Journal of Computer Engineering*, *14*(6), pp. 80–83. doi: https://doi.org/10.9790/0661-1468083

Moore, P. A., Lukenbach, M. C., Thompson, D. K., Kettridge, N., Granath, G., & Waddington, J. M. (2019). Assessing the peatland hummock-hollow classification framework using high-resolution elevation models: Implications for appropriate complexity ecosystem modeling. *Biogeosciences*, *16*(18), pp. 3491–3506. doi: https://doi.org/10.5194/bg-16-3491-2019

Nilsson, M. (2002). Mire Ecosystems. *Encyclopedia of Life Sciences*. doi: https://doi.org/10.1038/npg.els.0003194

Nungesser, M. K. (2003). Modelling microtopography in boreal peatlands: Hummocks and hollows. *Ecological Modelling*, 165(2–3), pp.175–207. doi: https://doi.org/10.1016/S0304-3800(03)00067-X

Pouliot, R., Rochefort, L., & Karofeld, E. (2011). Initiation of microtopography in revegetated cutover peatlands. *Applied Vegetation Science*, 14(2), pp. 158–171. doi: https://doi.org/10.1111/j.1654-109X.2010.01118.x

Rydin, H., & Jeglum, J. K. (2015). The Biology of Peatlands. *The Biology of Peatlands*. doi: https://doi.org/10.1093/acprof:osobl/9780199602995.001.0001

Rydin, H., Snoeijs, Pauli., Diekmann, Martin., & Maarel, E. van der. (1999). Swedish plant geography. *Svenska Växtgeografiska Sällskapet*

Shi, X., Thornton, P. E., Ricciuto, D. M., Hanson, P. J., Mao, J., Sebestyen, S. D., Griffiths, N. A., & Bisht, G. (2015). Representing northern peatland microtopography and hydrology within the Community Land Model. *Biogeosciences*, *12*(21), pp. 6463–6477. doi: https://doi.org/10.5194/bg-12-6463-2015

Sibaruddin, H. I., Shafri, H. Z. M., Pradhan, B., & Haron, N. A. (2018). Comparison of pixel-based and object-based image classification techniques in extracting information from UAV imagery data. *IOP Conference Series: Earth and Environmental Science*, *169*(1). doi: https://doi.org/10.1088/1755-1315/169/1/012098

Stovall, A. E. L., Diamond, J. S., Slesak, R. A., McLaughlin, D. L., & Shugart, H. (2019). Quantifying wetland microtopography with terrestrial laser scanning. *Remote Sensing of Environment*, *232*. doi: https://doi.org/10.1016/j.rse.2019.111271

Szporak-Wasilewska, S., Piórkowski, H., Ciężkowski, W., Jarzombkowski, F., Sławik, Ł., & Kopeć, D. (2021). Mapping alkaline fens, transition mires and quaking bogs using airborne hyperspectral and laser scanning data. *Remote Sensing*, *13*(8). doi: https://doi.org/10.3390/rs13081504

Villoslada, M., Bergamo, T. F., Ward, R. D., Burnside, N. G., Joyce, C. B., Bunce, R. G. H., & Sepp, K. (2020). Fine scale plant community assessment in coastal meadows using UAV based multispectral data. *Ecological Indicators*, *111*. doi: https://doi.org/10.1016/j.ecolind.2019.105979

Wang, L., & Liu, H. (2006). An efficient method for identifying and filling surface depressions in digital elevation models for hydrologic analysis and modelling. *International Journal of Geographical Information Science*, *20*(2), pp. 193–213. doi: https://doi.org/10.1080/13658810500433453

Wu, Y., & Blodau, C. (2013). PEATBOG: A biogeochemical model for analyzing coupled carbon and nitrogen dynamics in northern peatlands. *Geoscientific Model Development*, 6(4), pp. 1173–1207. doi: https://doi.org/10.5194/gmd-6-1173-2013

Xiang, T.-Z., Xia, G.-S., & Zhang, L. (2018). Mini-UAV-based Remote Sensing: Techniques, Applications and Prospectives. *IEEE Geoscience and Remote Sensing Magazine*, 7(3), pp. 29–63. doi: https://doi.org/10.1109/MGRS.2019.2918840

Yu, Z., Loisel, J., Brosseau, D. P., Beilman, D. W., & Hunt, S. J. (2010). Global peatland dynamics since the Last Glacial Maximum. *Geophysical Research Letters*, 37(13). doi: https://doi.org/10.1029/2010GL043584

Zayed, N., & Elnemr, H. A. (2015). Statistical Analysis of Haralick Texture Features to Discriminate Lung Abnormalities. *International Journal of Biomedical Imaging*. doi: https://doi.org/10.1155/2015/267807

Software:

AgiSoft Metashape Professional (Version 2.0.0) (Software). (2022*). Retrieved from: http://www.agisoft.com/downloads/installer/

Conrad, O., Bechtel, B., Bock, M., Dietrich, H., Fischer, E., Gerlitz, L., Wehberg, J., Wichmann, V., and Böhner, J. (2015): System for Automated Geoscientific Analyses (SAGA) v. 2.1.4, Geosci. Model Dev., 8, 1991-2007. doi: 10.5194/gmd-8-1991-2015

Guanter, L., Kaufmann, H., Segl, K., Foerster, S., Rogass, C., Chabrillat, S., Kuester, T., Hollstein, A., Rossner, G., Chlebek, C., Straif, C., Fischer, S., Schrader, S., Storch, T., Heiden, U., Mueller, A., Bachmann, M., Mühle, H., Müller, R., Habermeyer, M., Ohndorf, A., Hill, J., Buddenbaum, H., Hostert, P., van der Linden, S., Leitão, P., Rabe, A., Doerffer, R., Krasemann, H., Xi, H., Mauser, W., Hank, T., Locherer, M., Rast, M., Staenz, K., Sang, B. (2015). The EnMAP Spaceborne Imaging Spectroscopy Mission for Earth Observation. *Remote Sens.*, 7(7), pp. 8830-8857. doi: 10.3390/rs70708830

Grizonnet, M., Michel, J., Poughon, V., Inglada, J., Savinaud, M., & Cresson, R. (2017). Orfeo ToolBox: open source processing of remote sensing images. *Open Geospatial Data, Software and Standards*, *2*(1). doi: https://doi.org/10.1186/s40965-017-0031-6

QGIS Development Team, 2023.QGIS Geographic Information System. Open Source Geospatial Foundation Project. Retrieved from: http://www.qgis.org/

R Core Team, 2023. R: A language and environment for statistical computing. R Foundation for Statistical Computing, Vienna, Austria. Retrieved from: https://www.R-project.org/

Spyder Doc Contributors, 2023. Spyder-documentation. Retrieved from: *https://docs.spyder-ide.org/current/index.html*

Appendices

Appendix I: Microtopography class 3 evaluation

The absolute height of the hummock- like features in hollows (Hu.i.Ho.) (a2) and the absolute depth of hollows-like depressions on hummocks (Ho.o.Hu.) (b1) presented in Figure 6 point out, that the greater proportion of pixels are of very low value. The elevational classes on the x-axis are displayed in meters meaning that class 0.01, which by far has the most pixel counts in each four graphs, only shows elevational values of about 1 cm. For elevational classes above 1 cm the pixel counts constantly decrease with increasing class values. The last class represents the upper elevational thresholds, that differ slightly between each graph. It shows the broadest range of all classes and overall very low numbers in pixel count.

Considering the feature height and depth values as well as the overall spatial distribution of each elevational class, rejecting a separate class three was the most reasonable option in this case. Instead all class three pixels were either merged to the classes hummock or hollow by using a spatial index as described in the methods part. Hollow like structures are now considered as hollows when their absolute depth exceeds or equals the distance to the filled surface as pointed out in Figure 4. Hummocky areas in hollows become hummocks when their absolute height is bigger or equal to their distance to the filled surface (figure 4). The differences between the four-class modeling step and the final result with three classes are shown for a small extend around the Degerö flux tower in map one. The majority of the pixels were assigned to the surrounding feature forms. However, smaller pixel clusters can be found whose absolute height or depth was sufficient to form hummocks in hollows or hollows on hummocks. The final modelling workflow accessible through the GitHub link stated in section 2.3 passes the option to the user to either keep or reject class 3 depending on the overall modelling goal.

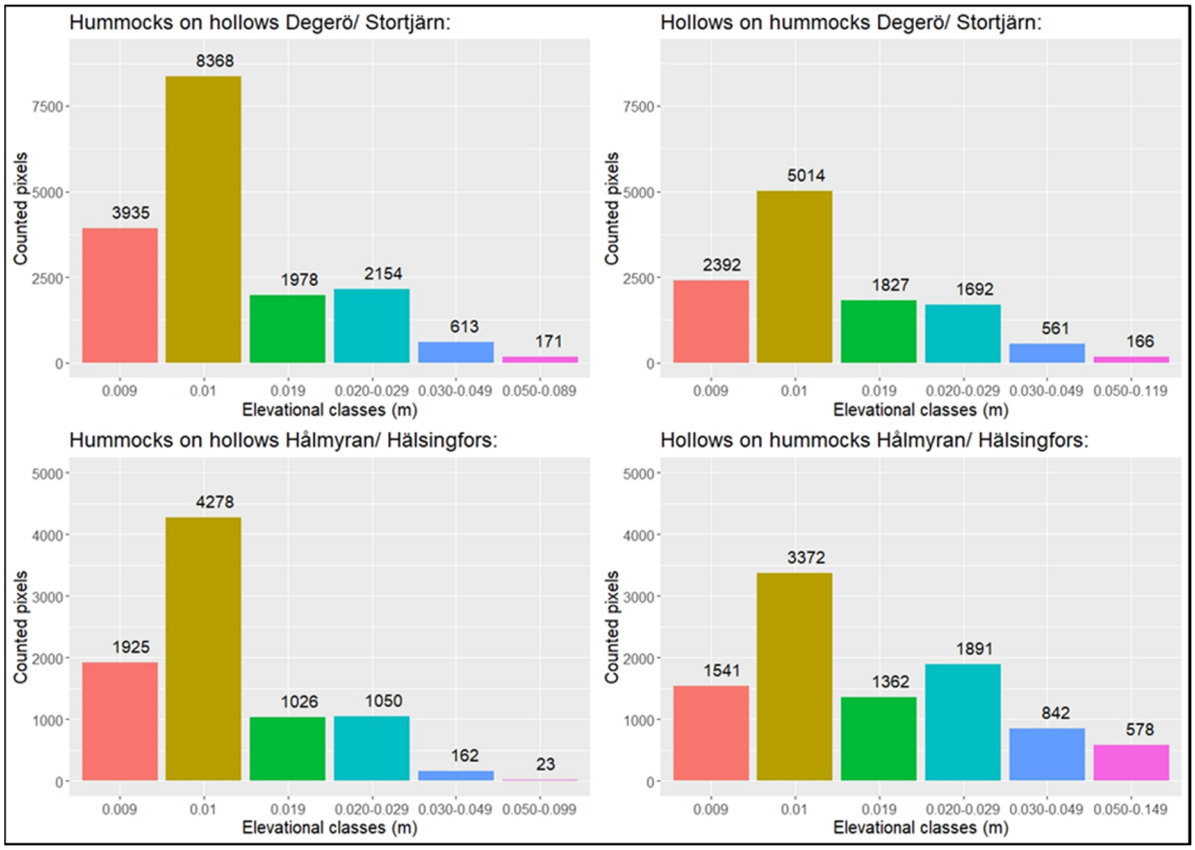

Figure A Absolute height and depth distribution of hummock- like features in hollows (Hu.i.Ho.) and hollow- like features on hummocks (Ho.o.Hu.). Graphicly illustrated in Figure 4.

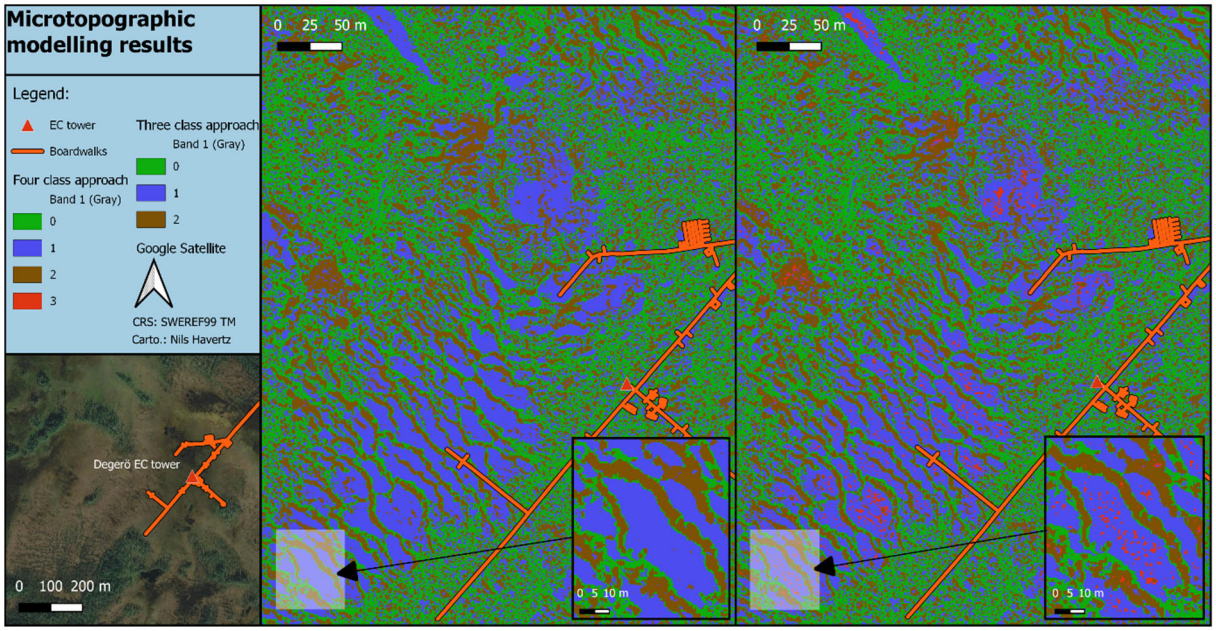

Figure B Comparison between the four- class and three- class modelling approach

Appendix II: Error matrices for vegetation classification

A. Confusion matrix Degerö with microtopography and DEM input parameters

	Predicted									
Classified		1	2	3	4	5	6	7	Totals	UA
	1	10455	560	6	2286	2448	35	0	15790	0.6621
	2	625	13014	178	668	1912	2	0	16399	0.7936
	3	25	146	9920	18	606	0	0	10715	0.9258
	4	593	0	0	30983	5573	11	0	37160	0.8338
	5	17	0	0	1863	94230	0	0	96110	0.9804
	6	198	43	0	488	162	1458	0	2349	0.6207
	7	0	0	2	0	21	0	4	27	0.1481
	Totals	11913	13763	10106	36306	104952	1506	4	178550	
	PA	0.8776	0.9456	0.9816	0.8534	0.8978	0.9681	1		
							OA	0.8964	Kappa	0.8342

B. Confusion matrix Degerö without microtopography and with DEM input parameters

	Predicted									
Classified		1	2	3	4	5	6	7	Totals	UA
	1	9886	607	3	2916	2347	31	0	15790	0.6261
	2	674	12666	256	891	1910	2	2	16401	0.7723
	3	29	162	9893	18	613	0	0	10715	0.9233
	4	601	2	0	30979	5567	11	0	37160	0.8337
	5	6	0	0	1969	94135	0	0	96110	0.9795
	6	219	52	0	501	109	1468	0	2349	0.6249
	7	0	0	4	0	19	0	4	27	0.1481
	Totals	11415	13489	10156	37274	104700	1512	6	178552	
	PA	0.8661	0.9390	0.9741	0.8311	0.8991	0.9709	0.6667		
							OA	0.8906	Kappa	0.825

C. Confusion matrix Degerö with microtopography without DEM input parameters

	Predicted									
Classified		1	2	3	4	5	6	7	Totals	UA
	1	10516	1137	96	1133	2872	36	0	15790	0.6660
	2	1619	11507	109	1294	1868	2	0	16399	0.7017
	3	446	141	9170	53	905	0	0	10715	0.8558
	4	1297	1697	3	19672	14465	26	0	37160	0.5294
	5	15	80	12	564	95439	0	0	96110	0.9930
	6	0	2	2	3	738	1604	0	2349	0.6828
	7	0	0	0	0	21	0	6	27	0.2222
	Totals	13893	14564	9392	22719	116308	1668	6	178550	
	PA	0.7569	0.7901	0.9764	0.8659	0.8206	0.9616	1.0000		
							OA	0.8284	Kappa	0.7165

D. Confusion matrix Degerö without microtopography and DEM input parameters

	Predicted									
Classified		1	2	3	4	5	6	7	Totals	UA
	1	10464	1468	96	901	2827	34	0	15790	0.6627
	2	1779	9547	103	2645	2323	2	0	16399	0.5822
	3	452	81	8955	204	1023	0	0	10715	0.8357
	4	1235	1737	41	18284	15839	24	0	37160	0.4920
	5	14	73	20	457	95546	0	0	96110	0.9941
	6	0	0	4	5	702	1638	0	2349	0.6973
	7	0	0	6	0	17	0	4	27	0.1481
	Totals	13944	12906	9225	22496	118277	1698	4	178550	
	PA	0.7504	0.7397	0.9707	0.8128	0.8078	0.9647	1.0000		
							OA	0.8089	Kappa	0.6818

E. Confusion matrix Stortjärn with microtopography and DEM input parameters

	Predicted									
Classified	Class	1	2	3	4	5	6	7	Totals	UA
	1	15119	20	0	97	276	0	0	15512	0.9747
	2	58	1993	2	306	1570	0	0	3929	0.5073
	3	0	71	214	13	75	0	0	373	0.5737
	4	489	21	0	16221	10849	0	0	27580	0.5881
	5	1211	24	0	1533	50089	4	0	52861	0.9476
	6	0	0	0	4	25	649	0	678	0.9572
	7	0	0	0	0	0	0	3	3	1.0000
	Totals	16877	2129	216	18174	62884	653	3	100936	
	PA	0.8958	0.9361	0.9907	0.8925	0.7965	0.9939	1.0000		
							OA	0.835	Kappa	0.7241

F. Confusion matrix Stortjärn without microtopography and with DEM input parameters

	Predicted									
Classified		1	2	3	4	5	6	7	Totals	UA
	1	15120	22	0	96	274	0	0	15512	0.9747
	2	65	2034	2	314	1514	0	0	3929	0.5177
	3	0	57	214	24	78	0	0	373	0.5737
	4	512	21	0	16233	10814	0	0	27580	0.5886
	5	1236	31	0	1517	50072	5	0	52861	0.9472
	6	0	0	0	5	24	649	0	678	0.9572
	7	0	0	0	0	0	0	3	3	1.0000
	Totals	16933	2165	216	18189	62776	654	3	100936	
	PA	0.8929	0.9395	0.9907	0.8925	0.7976	0.9924	1.0000		
							OA	0.835	Kappa	0.725

G. Confusion matrix Stortjärn with microtopography without DEM input parameters

	Predicted									
Classified		1	2	3	4	5	6	7	Totals	UA
	1	15096	23	0	114	279	0	0	15512	0.9732
	2	33	1984	2	166	1744	0	0	3929	0.5050
	3	0	71	215	10	77	0	0	373	0.5764
	4	660	33	0	10487	16384	16	0	27580	0.3802
	5	1115	33	0	1723	49988	2	0	52861	0.9456
	6	0	0	0	6	18	654	0	678	0.9646
	7	0	0	0	0	0	0	3	3	1.0000
	Totals	16904	2144	217	12506	68490	672	3	100936	
	PA	0.8930	0.9254	0.9908	0.8386	0.7299	0.9732	1.0000		
							OA	0.7770	Kappa	0.6183

H. Confusion matrix Stortjärn without microtopography and DEM input parameters

	Predicted									
Classified		1	2	3	4	5	6	7	Totals	UA
	1	15088	22	0	115	287	0	0	15512	0.9727
	2	31	1846	1	180	1871	0	0	3929	0.4698
	3	0	63	214	13	83	0	0	373	0.5737
	4	689	31	0	10135	16706	19	0	27580	0.3675
	5	1128	32	0	1773	49927	1	0	52861	0.9445
	6	0	0	0	4	19	655	0	678	0.9661
	7	0	0	0	0	0	0	3	3	1.0000
	Totals	16936	1994	215	12220	68893	675	3	100936	
	PA	0.8909	0.9258	0.9953	0.8294	0.7247	0.9704	1.0000		
							OA	0.7715	Kappa	0.6079

I. Confusion matrix Hålmyran with microtopography and DEM input parameters

	Predicted									
Classified		1	2	3	4	5	6	7	Totals	UA
	1	11040	198	0	397	275	0	0	11910	0.9270
	2	922	5168	30	1504	408	0	0	8032	0.6434
	3	0	101	2326	271	137	0	0	2835	0.8205
	4	326	43	1	29484	2402	1	0	32257	0.9140
	5	826	7	0	5718	37058	0	0	43609	0.8498
	6	0	0	0	9	4	640	0	653	0.9801
	7	0	0	0	0	0	0	4	4	1.0000
	Totals	13114	5517	2357	37383	40284	641	4	99300	
	PA	0.8418	0.9367	0.9868	0.7887	0.9199	0.9984	1.0000		
							OA	0.8632	Kappa	0.7984

J. Confusion matrix Hålmyran without microtopography and with DEM input parameters

	Predicted									
Classified		1	2	3	4	5	6	7	Totals	UA
	1	11102	189	0	362	257	0	0	11910	0.9322
	2	908	5038	29	1720	337	0	0	8032	0.6272
	3	0	83	2301	317	134	0	0	2835	0.8116
	4	330	49	0	29515	2363	0	0	32257	0.9150
	5	833	13	0	6678	36085	0	0	43609	0.8275
	6	0	0	0	14	0	639	0	653	0.9786
	7	0	0	0	0	0	0	4	4	1.0000
	Totals	13173	5372	2330	38606	39176	639	4	99300	
	PA	0.8428	0.9378	0.9876	0.7645	0.9211	1.0000	1.0000		
							OA	0.8528	Kappa	0.7833

K. Confusion matrix Hålmyran with microtopography without DEM input parameters

	Predicted									
Classified		1	2	3	4	5	6	7	Totals	UA
	1	10996	208	0	459	247	0	0	11910	0.9233
	2	1508	4822	69	838	795	0	0	8032	0.6003
	3	10	176	2049	332	268	0	0	2835	0.7228
	4	457	21	1	28410	3368	0	0	32257	0.8807
	5	794	115	10	6985	35702	3	0	43609	0.8187
	6	0	0	0	11	4	638	0	653	0.9770
	7	0	0	0	0	0	0	4	4	1.0000
	Totals	13765	5342	2129	37035	40384	641	4	99300	
	PA	0.7988	0.9027	0.9624	0.7671	0.8841	0.9953	1.0000		
							OA	0.8320	Kappa	0.7525

L. Confusion matrix Hålmyran without microtopography and DEM input parameters

	Predicted									
Classified		1	2	3	4	5	6	7	Totals	UA
	1	11010	205	0	471	224	0	0	11910	0.9244
	2	1464	4483	40	1282	763	0	0	8032	0.5581
	3	7	132	1933	471	292	0	0	2835	0.6818
	4	504	34	0	28359	3360	0	0	32257	0.8792
	5	837	97	11	8062	34599	3	0	43609	0.7934
	6	0	0	0	10	5	638	0	653	0.9770
	7	0	0	0	0	0	0	4	4	1.0000
	Totals	13822	4951	1984	38655	39243	641	4	99300	
	PA	0.7966	0.9055	0.9743	0.7336	0.8817	0.9953	1.0000		
							OA	0.8160	Kappa	0.7288

M. Confusion matrix Hälsingfors with microtopography and DEM input parameters

	Predicted								
Classified		1	2	3	4	5	6	Totals	UA
	1	14509	1453	249	2718	496	0	19425	0.7469
	2	1338	12741	2080	1660	545	0	18364	0.6938
	3	2478	2399	40382	56	182	0	45497	0.8876
	4	468	198	433	24660	1876	0	27635	0.8923
	5	79	107	685	3933	34422	0	39226	0.8775
	6	0	0	0	122	0	667	789	0.8454
	Totals	18872	16898	43829	33149	37521	667	150936	
	PA	0.7688	0.7540	0.9214	0.7439	0.9174	1.0000		
						OA	0.8439	Kappa	0.7993

N. Confusion matrix Hälsingfors without microtopography and with DEM input parameters

	Predicted								
Classified		1	2	3	4	5	6	Totals	UA
	1	13961	1489	243	3158	574	0	19425	0.7187
	2	1245	11610	2388	2606	515	0	18364	0.6322
	3	3165	2074	39943	133	182	0	45497	0.8779
	4	416	141	464	24732	1882	0	27635	0.8950
	5	71	54	739	4075	34287	0	39226	0.8741
	6	1	0	0	100	0	688	789	0.8720
	Totals	18859	15368	43777	34804	37440	688	150936	
	PA	0.7403	0.7555	0.9124	0.7106	0.9158	1.0000		
						OA	0.8296	Kappa	0.7808

O. Confusion matrix Hälsingfors with microtopography without DEM input parameters

	Predicted								
Classified		1	2	3	4	5	6	Totals	UA
	1	13346	1478	877	2130	1594	0	19425	0.6871
	2	1810	8320	4563	1516	2155	0	18364	0.4531
	3	1261	2206	40116	1049	865	0	45497	0.8817
	4	1109	116	178	22119	4101	12	27635	0.8004
	5	162	264	1946	3834	33015	5	39226	0.8417
	6	0	0	36	62	1	690	789	0.8745
	Totals	17688	12384	47716	30710	41731	707	150936	
	PA	0.7545	0.6718	0.8407	0.7203	0.7911	0.9760		
						OA	0.7792	Kappa	0.7134

P. Confusion matrix Hälsingfors without microtopography and DEM input parameters

	Predicted								
Classified		1	2	3	4	5	6	Totals	UA
	1	13134	1431	1411	1985	1464	0	19425	0.6761
	2	2400	7496	4460	1777	2231	0	18364	0.4082
	3	1745	2080	38880	1774	1016	2	45497	0.8546
	4	1373	302	605	19277	6073	5	27635	0.6976
	5	155	217	2288	3945	32620	1	39226	0.8316
	6	0	0	39	47	0	703	789	0.8910
	Totals	18807	11526	47683	28805	43404	711	150936	
	PA	0.6984	0.6504	0.8154	0.6692	0.7515	0.9887		
						OA	0.7428	Kappa	0.6658

Appendix III: Comparison between mapping results of microtopography and vegetation classification along a Degerö boardwalk extend

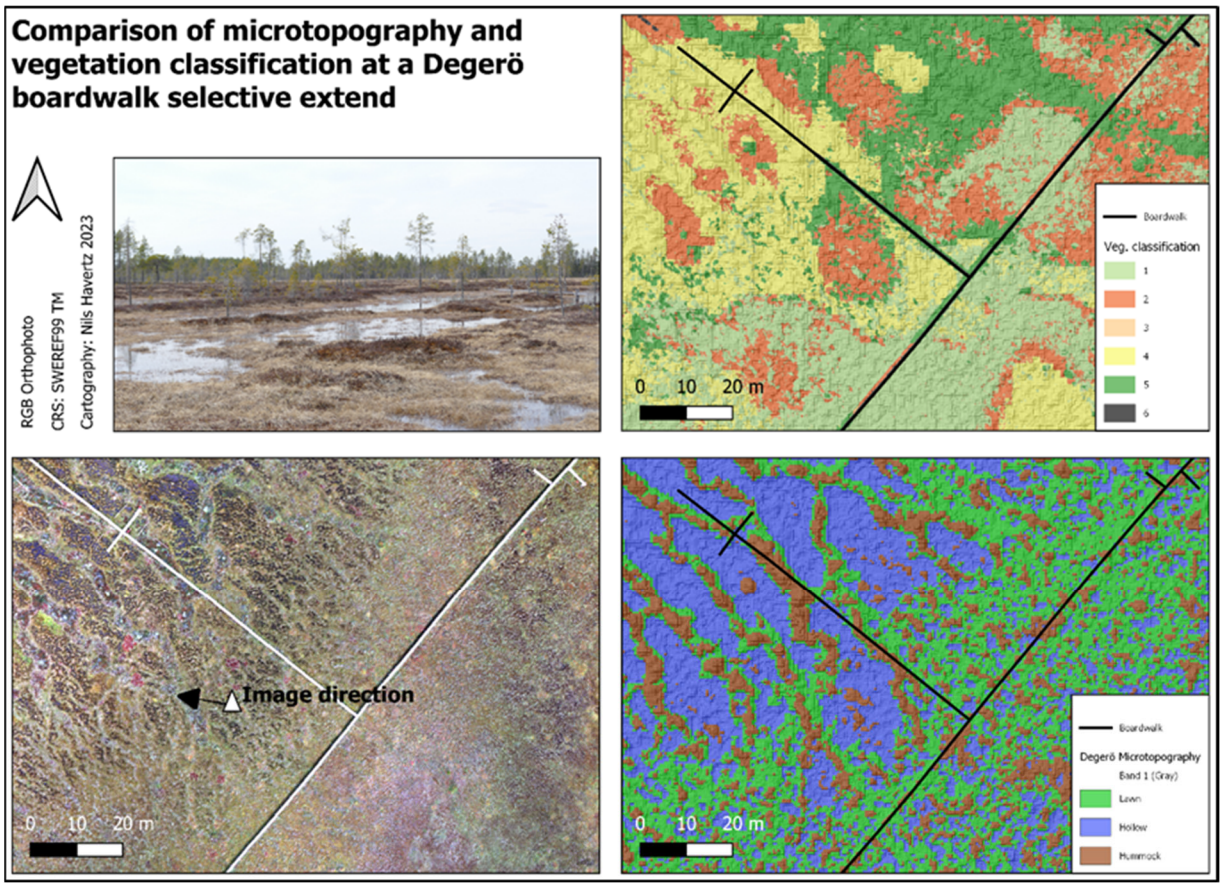

Figure A Comparison between microtopographic modeling results, vegetation classification results including all parameters (Spectral, microtopography and DEM), true color composite from drone imagery and a picture taken in field for a small extend at the end of the Degerö Stormyr boardwalk.

Publishing and archiving

Approved students' theses at SLU are published electronically. As a student, you have the copyright to your own work and need to approve the electronic publishing. If you check the box for **YES**, the full text (pdf file) and metadata will be visible and searchable online. If you check the box for **NO**, only the metadata and the abstract will be visible and searchable online. Nevertheless, when the document is uploaded it will still be archived as a digital file. If you are more than one author, the checked box will be applied to all authors. You will find a link to SLU's publishing agreement here:

- https://libanswers.slu.se/en/faq/228318.

☒ YES, I/we hereby give permission to publish the present thesis in accordance with the SLU agreement regarding the transfer of the right to publish a work.

☐ NO, I/we do not give permission to publish the present work. The work will still be archived and its metadata and abstract will be visible and searchable.

SENASTE UTGIVNA NUMMER

2022:06 Författare: Louise Nordström
Growth and development of Eucalyptus grandis seedlings in response to arginine phosphate application

2022:07 Författare: Alice Falk
Towards climate optimised riparian buffer zones in boreal forests. Investigation of clearcutting effects on soil temperature, soil moisture and greenhouse gas fluxes in riparian buffer zones with different widths

2022:08 Författare: Pelle Kronborg
Biogeochemistry and Peat Properties of Restored Peatlands

2022:09 Författare: Andreas Souropetsis
Influence of forest mires on wildfire
A landscape analysis of the 2014 Västmanland forest fire

2022:10 Författare: Leon Hauenschild
Alteration of the forest structure in historically impacted Nothofagus spp. forests on the Brunswick peninsula.
Recommendations for their protection and management.

2022:11 Författare: Axel Strömberg
The evaluation of novelty kilns: drying msasa wood at a small scale sawmill in Mozambique

2022:12 Författare: Andreas Karlstrand
Samband mellan föryngringsresultatet år 5 och kvalitetsklassning av markberedning och planteringsåtgärder på SCA:s fasta provytor i norra Sverige.

2023:01 Författare: Tyra Tornberg
Forest regeneration and edge effects – An ecophysiological analysis after gap-cutting

2023:02 Författare: Erik Wickberg
Effekten av växtnäring på överlevnad, tillväxt och vitalitet på planterade tall- och granplantor - En studie gjord på ett kontrollerat försök på en lokal i Västerbotten

2023:03 Författare: Carl Åhlund
Kvävegödslingens effekter på bladyta och trädkronor i tallbestånd

2023:04 Författare: Johan Engström
Increased carbon sequestration of actively restored tropical forests in Sabah, Malaysia
A comparison of natural regeneration and active restoration

2023:05 Författare: Magdalena Fassl
Tree-growth and climate-growth relationships of Scots pine and downy birch in a natural forest in northern Sweden

2023:06 Författare: Ruben Baan Hofman
Riparian vegetation ecology
An observational study into the effects of forest management on understory vegetation communities along boreal headwaters

2023:07 Författare: Nils Helge Havertz
GIS and remote sensing based mapping of microtopography and vegetation composition in a boreal mire complex